Likelihood free and likelihood based approaches to modeling and analysis of functional antibody titers with applications to group B Streptococcus vaccine development.

PhD thesis of Luca Moraschini

University of Milano-Bicocca, department of Health Sciences

PhD supervisors: Giovanni Corrao

Novartis supervisor: Fabio Rigat

Chapter 3: Bayesian modeling of integrated threshold free functional antibody titers

Chapter 1 Introduction: Group B Streptococcus and Immunoassays

Streptococcus agalactiae (Group B *streptococcus*, GBS) is a haemolytic, encapsulated Gram-positive bacterium colonizing the ano-genital tract of 25-30% healthy women [1]. GBS is a major cause of early (EOD) and late (LOD) onset neonatal infection leading to neonatal pneumonia, sepsis and meningitis causing 4-10% mortality and long-term disability [2]. GBS is also increasingly recognized as an important cause of disease in adults, particularly those with underlying disease, and in the elderly [3,4]

Antenatal screening and intra-partum antibiotic prophylaxis for GBS colonized women has substantially reduced incidence of GBS neonatal infection [5-7]. Due to the causal link between maternal antibody deficiency and susceptibility to GBS neonatal infection, the development of safe and effective GBS vaccines remains to date the most promising strategy for preventing group B streptococcal disease [8-9]. Antibodies are glycoproteins, also called Immunoglobulin, produced by the human adaptive immune system in response to the introduction of a dangerous external pathogen, such as bacteria, virus or fungi. The antibodies specifically have the ability to bind the *antigens*, molecules typically expressed on the pathogen surface, and help the process of eliminations of these dangerous elements. Antibodies can be divided in 5 different classes: IgG, IgM, IgA, IgD and IgE according to their different chemical composition. Specifically, maternal IgG antibodies against the bacterial capsular polysaccharide are known to correlate with a serotype specific reduction of disease risk in the newborns [10-12]. Since protective immunity to the ten capsular polysaccharide structural variants (Ia, Ib, II, III, IV, V, VI, VII, VIII, IX) is serotype-specific, vaccination of pregnant

women using epidemiologically relevant GBS capsular polysaccharides could be a successful strategy to defeat GBS neonatal disease. Safety and immunogenicity of GBS capsular polysaccharide investigational vaccines in healthy adults with and without conjugation to carrier proteins has been extensively investigated since the 1980s [13-16]. These studies mostly rely on accurate measures of serum concentration of vaccine-induced antibodies, which is a crucial issue in vaccine development. The quantification of vaccine-induced serum antibodies is performed using *immunoassays* [17]. An immunoassay is a biochemical test having the goal to quantify and measure the presence of a macromolecule within a solution using antibodies [18]. Usually, the macromolecule of interest is the antigen, and the solution is the blood serum. However, in many cases the role of antigen-antibodies is switched, and consequently through the use of antigens the immunoassay quantifies the presence of antibodies.

Immunoassays may be classified in two groups: non-functional and functional [17-19]. Non-functional assays are experiments in which the goal is to directly quantify the antibody concentration in a serum sample. The non-functional immunoassay most widely used is the Enzime-Linked Immunosorbent Assay (ELISA) [20]. Functional immunoassays differ from non-functional because they do not quantify the amount of serum antibodies, but their functionality in the serum. Although antibody serum concentration as measured by ELISA informs on the adaptive immune system response to vaccination, its contribution to predicting potential vaccine efficacy is confounded by the natural variability of the functional profile of the vaccine-raised antibodies.

Since adaptive immunity against GBS is mediated by opsonin-dependent phagocytosis [21,22], an in-vitro assay suitable to estimating functional

bactericidal activity of GBS-immunized sera is the better candidate for the vaccine development. Opsonin-dependent phagocytosis is the mechanism through which the immune system kills foreign particles or living pathogens through ingestion by phagocytes (monocytes, macrophages, neutrophils, dendritic and mast cells [23]). The opsonisation is an antibody-dependent mechanism through which the phagocytic process is enhanced and therefore it is called opsonophagocytosis. This mechanism plays a key role in the immune system.

The opsonophagocytosis killing assay (OPKA) is the functional assay that mimics the *in vivo* process of killing by host effector cells, following opsonisation by specific antibodies [24-26,39] (Figure 1.1 below). OPKA measures the extent to which bacteria are up-taken by phagocyte cells and killed when confronted with blood serum through opsonisation. The experimental components of OPKA comprise effector cells (e.g. human leukocytes), buffer, blood serum, complement and bacteria. Opsonophagocytic cells are suspended in buffer and aliquoted in different wells. A complement-deactivated blood serum is added, together with a bacterial suspension and a rabbit complement. Then the reaction runs for 45 minutes. The opsonophagocytosis is quantified using the number of bacteria (Colony Forming Unit counts or CFU) before and after the reaction. Alternatively, opsonophagocytosis can be quantified by contrasting the CFU counts measured after the reaction with that of a control experiment not exposing the bacteria to the test serum. The quantification of antibodies mediating killing of target pathogens in human serum samples is a cornerstone of many vaccine research and development programs [1,40-41].
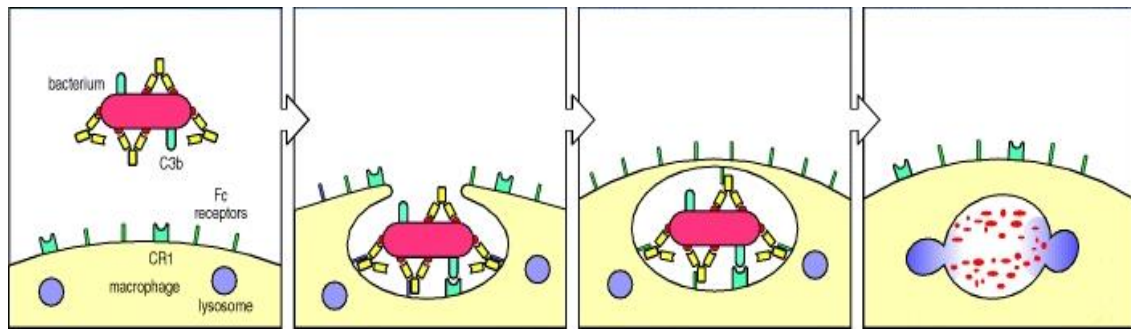
Figure 1.1: illustrative vignette of the OPKA assay biology

The primary OPKA readouts is called *titers*. A titer is a one-dimensional summary of a dose-response curve conveying biological and clinical interpretability. As such, no titer definition can capture *all potentially relevant differences* across the dose-response curves of different biological samples. However, a titer can provide an *appropriate* tool for decision-making to the extent that it detects biologically interpretable and clinically relevant differences across broadly different dose-response curves. OPKA titers are estimated by applying two data dimensionality reductions to the raw readouts (CFU counts) of serial dilutions experiments. First, the CFU counts prior to and after the bactericidal activity at each serum dilution are combined into the killing statistic. Second, the dilution-killing curve is fitted using a non-linear dose-response regression model and the titer is defined as the maximum serum dilution associated to a predefined bacterial killing threshold value. The choice of a threshold value and of a statistical model for titer estimation in functional immunoassays such as OPKA represents a source of *technical* variability that in principle can hinder the comparison of different clinical trials results [27].

The goal of this thesis is to provide more precise methods for titer estimation, using a two-step approach: first a threshold and likelihood free approach will be presented providing an robust tool to analyse OPKA data and amenable to being

easily implemented into routinely OPKA data analysis also from researchers who are not familiar with statistical modeling and language. Second, a likelihood-based approach will be presented in order to fully articulate the threshold free approach to titer estimation by making explicit the mathematical bases of its definition and by investigating appropriate numerical tools to derive threshold-free titer estimates from experimental data. This generalisation confers methodological breath to the present thesis, addressing issues of titer identifiability, invariance to specific classes of data transformations and equivalence to threshold-based titers under linearity of the OPKA dose-response curve.

Since this approach relies on a full understanding of a wide range of statistical procedures, the implementation for the routinely OPKA analysis will likely be less straightforward compared to the likelihood-free methods illustrated in Chapter 2, due to the increased complexity of likelihood-based estimation for researchers who are not used to deal with statistical languages. This issue has heavily affected the structure and content of this work, mostly stimulating and challenging the Author constructively towards a better understanding of the role of the applied statistician. One key issue that emerged from this process is the need to develop specific tools for data analysis addressing in a timely fashion scientifically relevant issues and to be able to effectively communicate their added value compared to simple descriptive analyses beyond the technicalities. Efforts to accomplish this bridging between statistical modeling and the experimental sciences distinguish the applied from the mathematical statistician and are vital to raise the awareness of how much a statistical approach is relevant for daily experimental work and decision-making. In absence of such

effective efforts, the technical discussions about which model may be better to address a specific scientific question become meaningless because the statistician would not be sufficiently understood nor adequately respected.

Since these efforts comprised a substantial relational component beyond their scientific and technical contents, the ensuing learnings deserve a brief yet dedicated reflection, as an example of establishing a path towards successful collaboration. At the beginning of my PhD I proposed developing advanced statistical approaches, somewhat disregarding the importance of patterns in biological data routinely observed in the laboratory yet not formally modeled. However, within an environment that is not strong in statistical modeling, this approach initially resulted in scepticism towards my work. This led to the development of less complex techniques and to presenting their results in such a way as to emphasize their practical advantages rather than their methodological foundations. Not surprisingly, this approach resulted effective and radically improved the interactions with experimental researchers. As soon as these understood the utility of what we proposed, their willingness to interact and also to ponder the details of novel approaches to data analysis improved. Only after being successful in engaging the experimental collaborators it was possible to introduce more general methods leveraging on more advanced statistical models. It is worth emphasizing this issue this now, because it was one of the greatest and probably the most surprising achievements of this PhD work.

This thesis is organised as follows. Chapter 2 illustrates a novel titer definition not depending on any killing threshold or on a dose-response model. These titers are hereby referred to as *threshold-free* titers and are a tool that is a powerful candidate to become part of the routinely OPKA analysis. Precision and linearity

of traditional and threshold-free titers are compared using simulated data and group B Streptococcus OPKA experimental data. Simulated killing values were generated using a heteroskedastic four-parameter (4PL) logistic dose-response model [28]. The third Chapter of this thesis presents a methodological extension of threshold free titers. This extension is motivated by the need to better take into account those case in which the assay is saturated for physical limitations of the machinery (plateau). These titers are referred as *Integrated titers*. Integrated titers are estimated within the Bayesian framework, and the operational properties are evaluated first using an appropriate set of simulation scenarios and then using a set of experimental data testing the functionality of anti-GBS antibody in human samples collected by a European observational study. The fourth Chapter concludes this thesis with a critical appraisal of the results obtained so far and illustrating directions of ongoing and future research work.

CHAPTER 2 Threshold-free estimation of functional antibody titers of a group B Streptococcus opsonophagocytic killing assay[1]

This Chapter illustrates in detail how OPKA titers are currently estimated and a novel definition of functional antibody titers. Specifically, Section 2.1 illustrates the strengths and weaknesses of threshold-based titer quantification methods. Section 2.2 is dedicated to the definition of threshold-free titers. Section 2.3 presents the simulation study results, focussing on the comparison of the operational characteristics of threshold-free and threshold-based titers under four illustrative scenarios. Section 2.4 analyses a set of OPKA experimental data, contrasting assay precision and linearity under the two titer definitions. Section 2.5 concludes this Chapter providing a critical summary of its main results and describing relevant directions for further research.

2.1 Threshold-based estimation of OPKA titers

The bactericidal activity of the antibody in blood serum $i=1,...,I$ at the dilutions[2] $d_1 \leq d_2 \leq \cdots \leq d_J$, is quantified in OPKA using the number of colony forming units $CFU_{0,i}(d_j)$ and $CFU_{1,i}(d_j)$ for $j=1,...,J$ measured prior to (time t_0) and after (time t_1)

---

[1] Chapter adapted from "Threshold-free estimation of functional antibody titers of a group B Streptococcus opsonophagocytic killing assay", by L.Moraschini, I.Passalacqua, M.Fabbrini, I.Margarit Y Ros, F.Rigat. Forthcoming on Pharmaceutical Statistics, 2015

[2] Each dilution value d represents the inverse of the serum concentration used in an experiment. For instance, the $d=100$ means that the serum was diluted one-hundred fold in buffer prior to the start of the opsonophagocytic reaction.

the in vitro opsonophagocytic bactericidal reaction. These CFU counts are combined into the killing statistic

$$K_i(d_j) = 100 \times \frac{\mathrm{CFU}_{0,i}(d_j) - \mathrm{CFU}_{1,i}(d_j)}{\mathrm{CFU}_{0,i}(d_j)}.$$ (2.1)

The main strength of (2.1) lies in its biological interpretability, in that killing values comprised within the interval $(0,100)$ quantify a *net* decrease in the number of live bacteria at a given serum dilution and negative killing indicates *net* bacterial growth within the time interval (t_0, t_1). Its main operational limitation is that, being (2.1) bounded by construction within the interval $(-\infty, 100)$, the experimental variability of killing is typically dilution-dependent. The killing statistics (2.1) measures the *net* result of the increase in CFU count due to bacterial proliferation and its decrease to bacterial death between times t_0 and t_1. Alternatively, killing can be quantified by contrasting the CFU count measured at time t_1 with that of a control experiment not exposing the bacteria to the test serum. The titer definitions illustrated in this paper are applicable regardless of whether killing is measured using either of these two methods.

An alternative summary statistic of CFU counts that preserves biological interpretability is the log-ratio:

$$(d_j) = \mathrm{Log}_2\left(\frac{\mathrm{CFU}_{0,i}(d_j)}{\mathrm{CFU}_{1,i}(d_j)}\right) = -\mathrm{Log}_2\left(1 - \frac{K_i(d_j)}{100}\right).$$ (2.2)

This statistic is a real-valued monotone transformation of (2.1) taking high values when killing is high and vice versa. Due to its amenability to statistical

inference, the statistical model used in this work will be specified as a probability distribution of the log-ratio over different serum dilutions.

The threshold-based titer estimator for each serum i, hereby denoted as $T_{k^*,i}$, is defined as the maximum serum dilution within the interval $[d_1, d_J]$ such that the fitted killing curve $\widehat{K}_i(d)$ is greater or equal than a predefined threshold value k^*:

$$T_{k^*,i} = \max\{d : \widehat{K}_i(d_j) \geq k^*\}. \qquad (2.3)$$

The titer estimator (2.3) depends on the fixed threshold k^*, which is a killing value contained within the expected range of linearity of the killing curves of all tested sera. Consistently with common experimental practice, throughout this paper titers (2.3) are estimated using k^*= 50. However, when the killing curves of many sera are fitted over the same set of dilutions, the range of killing values where all curves are approximately linear in the dilution can be either null or it can be an interval. Therefore, in practice titers (2.3) are defined using a killing threshold that is either suboptimal or arbitrarily chosen within many equally suitable values. Also, since the number of tested serum dilutions is typically low, the dilution associated to this critical cut-off can be estimated precisely only by using an interpolating dose-response model. The simplest such model used in current practice is piece-wise linear interpolation (PWLI), which estimates the killing curve within $[d_1, d_J]$ by connecting with a segment the measured killing of each pair of tested dilutions. PWLI is simple, in that no statistical package is required to estimate titers. Its main limitation is that the values of titers (2.3) estimated by PWLI depend only on the two data points where the critical killing threshold is crossed. Also, when the killing curve does not cross its critical

threshold k^* or it crosses it at multiple dilutions, titers (2.3) are either undefined or not unique. These limitations are mitigated when estimating (2.3) using monotone dose-response models, so that all data points contribute to titer estimation and the only titer estimate exists when the fitted killing curve crosses the threshold k^*. These threshold-based titers do not need to lie within the range of tested dilutions $[d_1, d_J]$ as the fitted killing curve can be extrapolated beyond this range. Table 2.1 summarizes the operational attributes of titer estimates (2.3) under PWLI and monotone dose-response models. Biological interpretability, computational simplicity, uniqueness and dependence on all observed data are identified in Table 21..1 as strengths. However, lack of robustness arises as a result of the dependence on one killing threshold and on specific dose-response modelling assumptions.

Operational Attributes	Piece-wise Linear Interpolation	Monotone dose-response models
Threshold-independent	No	No
Extrapolation	No	Yes
Uniqueness	No	Yes
Computationally simple	Yes	No
Estimated using all data	No	Yes

Table 2.1: operational attributes of threshold-based titer estimates under PWLI and monotone dose-response models.

2.2 Threshold-free estimation of OPKA titers

A titer estimator having all attributes listed in Table 2.1 can be defined as a weighted average of the tested serum dilutions, with weights taken as functions of the associated killing values. For each serum i the *threshold-free* titer is defined as

$$T_{f,i} = \sum_{j=1}^{J} d_j w_{ij},\qquad(2.4)$$

with $w_{ij} \geq 0$ and $\sum_{j=1}^{J} w_{ij} = 1$. Here we investigate the operational characteristics of (2.4) when the weights w_{ij} are defined as the normalized non-negative killing values

$$w_{ij} = \frac{K_i(d_j)1_{\{K_i(d_j) \geq 0\}}}{\sum_{j=1}^{J} K_i(d_j)1_{\{K_i(d_j) \geq 0\}}}.\qquad(2.5)$$

These weights are normalized in (2.5) so as to ensure that the resulting estimates lie within the interval of tested dilutions $[d_1, d_J]$. Under (2.5), the threshold free titer estimator (2.4) is an average of the tested serum dilutions demonstrating antibody functionality against the bacteria (positive killing) weighted by the associated killing values. High threshold-free OPKA titers are indicative of persistent bactericidal activity of the serum antibody even when highly diluted. Also, while any set of killing curves crossing the critical threshold from above at the same dilution share the same titer (2.3), threshold-free titers

(2.4)-(2.5) are invariant to multiplication of all positive killing values by the same positive factor.

Threshold-free titers are sensitive to saturation of the killing curve either above (*left plateau*) or below (*right plateau*). In these cases, estimates of (2.4)-(2.5) can be skewed towards lower or higher dilution values respectively. This potential oversensitivity to assay saturation is prevented by generalizing the definition of the weights (2.5) as

$$w_{ij} = \frac{K_i(d_j)1_{\{K_i(d_j)\geq 0,\, d_g(z)\leq d_j \leq d_r(z)\}}}{\sum_{j=1}^{J} K_i(d_j)1_{\{K_i(d_j)\geq 0,\, d_g(z)\leq d_j \leq d_r(z)\}}}, \tag{2.6}$$

where the range of dilutions associated to non-zero weights becomes:

$$d_g(z) = \min_d(|K(d_k) - K(d_{k+1})| \geq z, k = 1, \dots, K-1),$$

$$d_r(z) = \max_d(|K(d_k) - K(d_{k+1})| \geq z, k = 1, \dots, K-1). \tag{2.7}$$

The *plateau condition* $z \in (0,100)$ in (2.6) and (2.7) represents the smallest biologically meaningful difference between killing values associated to successive serum dilutions. High values of z imply that only a small number of tested dilutions are used for estimating threshold-free titers. Therefore, plateau threshold-free titers ($_pT_f$) calculated using high z values tend to be less precise than estimates calculated under (2.5). In this paper we estimate threshold-free OPKA titers using z values within the range 0-20. Ideally, the values of z should be selected on a set of *ad-hoc* experiments designed to analytically quantify when a difference between successive killings is sufficient to exclude the

occurrence of plateaus. In practice, this exercise is almost impossible to perform due to many reasons, so we decide according to OPKA researchers to use the method using a biological rationale.

To illustrate the robustness of $_pT_f$ titers, Figure 2.1 displays one killing curve showing a long left plateau associated to high killing values (solid curve) and a second curve displaying a long right plateau associated to small and positive killing values (dashed curve). The T_{50} titers for the dashed and solid curves are 4.4 and 49.8 respectively, indicating higher antibody functionality for the solid curve. In contrast, the T_f titers for the dashed and solid curves are 40 and 21 respectively, indicating higher antibody functionality for the dashed curve. This result is biologically questionable because the solid curve exhibits much higher killing values through most of the range of tested dilutions. However, when threshold free titers are estimated using the plateau condition $z=5$ the $_pT_f$ titers are 7.8 and 26.1 for the dashed and solid curves respectively. Here $_pT_f$ estimates are calculated from six and four dilution/killing pairs for the solid (dilutions 8 through 256) and dashed (dilutions 4 through 32) curves respectively. Therefore, robustification against assay saturation ensures the biological interpretability of threshold free titers while preserving its ability to learn from the unsaturated portion of the killing curve.

Titer estimates left plateau (solid) and right plateau (dashed) killing curves

Legend:
- □ T_{50} PWLI dashed = 4.4
- ○ T_{50} PWLI solid = 49.8
- ■ T_f dashed = 40
- ● T_f solid = 21
- △ pT_f dashed = 7.8
- ▲ pT_f solid = 26.1
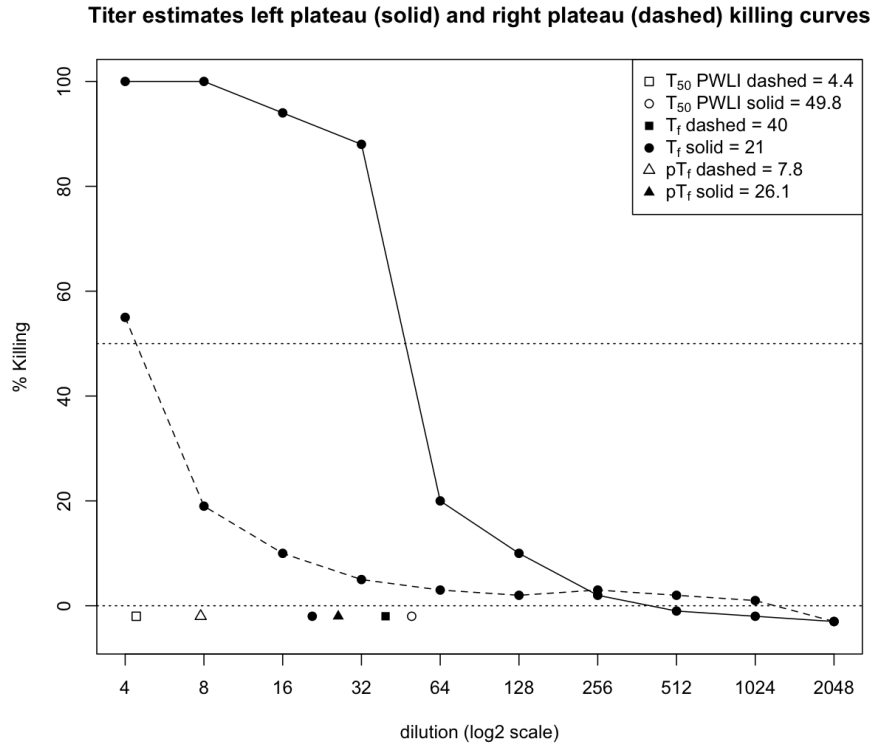
Figure 2.1: Plateau threshold free titers preserve biological interpretability when curves having long plateaus are confronted

2.3 Operating characteristics of threshold-based and threshold-free OPKA titers using simulated data

OPKA data were simulated under four scenarios *s=1,…,4*, encompassing the absence of saturation or "no plateau", constant killing at low serum dilutions or "left plateau" and constant killing at high serum dilutions or "right plateau". To this end, the log-ratio simulation model used was

$$LR_s(d_j, h) \sim N(LR_s(d_j), h * LR'_s(d_j)), \qquad (2.8)$$

where the mean log-ratio curve is taken as the 4PL logistic model:

$$LR_s(d_j) = LR(d_j, \alpha_s, \beta_s, \gamma_s, \delta_s) = \delta_s + \frac{\alpha_s - \delta_s}{1 + \left(\frac{d_j}{\gamma_s}\right)^{\beta_s}}.$$ (2.9)

Using (2.2), for each simulated log-ratio value the corresponding killing is:

$$K_s(d_j) = 100 \text{ x} \left(1 - 2^{-LR_s(d_j)}\right)$$ (2.10)

Model (2.8) makes sense for OPKA data because, like many other bioassays, OPKA presents saturation both above and below. This key feature of the assay is taken into account in equation (2.9) because δ_s and α_s are upper and lower asymptotes of the log-ratio curve. In addition, larger values of β_s correspond to steeper curves and larger values of γ_s shift the curves horizontally along the dilution axis [13]. The main drawback of this model lies in its weakly identifiability requiring the user to impose a constraint on whether alpha or delta represent the upper asymptote.

The parameter $h \geq 0$ in (2.8) defines the scale of the variance of the simulated data with larger h values corresponding to larger variances. Dose-response curves typically present a variability that is closely related to the sensitivity of the assay. Therefore, a convenient and appropriate way to define the variance in equation (2.8) is to multiply the scaling factor h for the first derivative of the 4PL mean function:

$$LR'_s(d_j) = \frac{-(\alpha_s - \delta_s)\beta_s (d_j)^{\beta_s - 1}}{\gamma_s^{\beta_s}\left(1 + \left(\frac{d_j}{\gamma_s}\right)^{\beta_s}\right)^2}.$$ (2.11)

The no plateau (s=1), one left plateau point (s=2), two left plateau points (s=3) and long right-plateau (s=4) scenarios were defined using the 4PL coefficient values

$$\alpha_1 = -5; \beta_1 = 1, \gamma_1 = 60; \delta_1 = 1.7,$$

$$\alpha_2 = -4; \beta_2 = 4; \gamma_2 = 120; \delta_2 = 1.5,$$

$$\alpha_3 = -2; \beta_3 = 4; \gamma_3 = 300; \delta_3 = 2,$$

$$\alpha_4 = -2; \beta_4 = 3; \gamma_4 = 70; \delta_4 = -0.3,$$

and the six common dilutions [30,60,120,240,480,960]. Figure 2.2 shows the corresponding non-negative killing values for each of the four simulation scenarios calculated from the 4PL log-ratio means of (2.8) using (2.10). The threshold-based titers (2.3) for scenarios s=1,...,4 are 89, 126, 228 and 79 whereas the threshold free titers T_f are 56, 63, 98 and 187 and the plateau threshold free titers $_pT_f$ using $z=5$ are 56, 83, 165 and 79. The T_f titers for scenarios 1-3 range from one third to one half of the corresponding T_{50} titers. As expected, the values of T_f and $_pT_f$ for scenario 1 coincide due to the absence of plateaus, whereas for scenarios 2 and 3 $_pT_f$ is closer to T_{50} values compared to T_f, with both threshold free titers yielding more conservative estimates of antibody functionality compared to T_{50}. For the right plateau scenario T_f is larger than T_{50} due to the long right tail of small and positive killing values. In this case the value of $_pT_f$ is much smaller than that of T_f demonstrating again the relevance of the plateau condition when estimating threshold free titers from partially saturated killing curves.
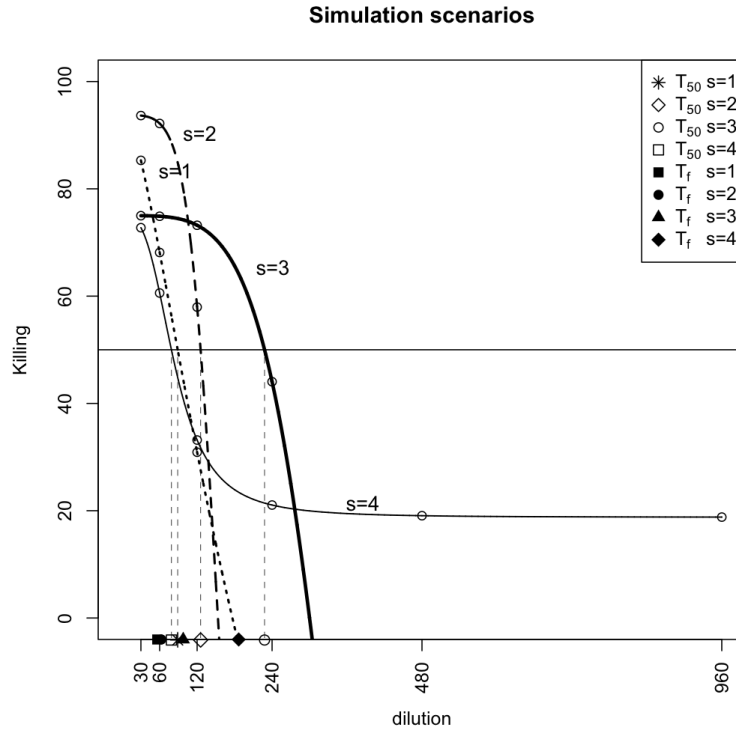
Figure 2.2: killing curves generated by different 4PL coefficients defining no plateau points (s=1), one left plateau point (s=2), two left plateau points (s=3) and long right plateau (s=4) scenarios.

Figure 2.3 shows the dilution-dependent standard deviations of the log-ratio (2.8) for each simulation scenario. Thick curves represent the dilution ranges associated to positive killing values. Empty circles mark the values of standard deviation associated to the six dilutions used for titer estimation. The one point left plateau scenario (s=2) exhibits the highest standard deviation at the third dilution, which is associated to the lowest positive killing value. In this case, the probability that its associated killing is negative under (2.8) is non-negligible so that this dilution value will be randomly included or excluded from (2.4) across simulations, leading to an increased variability of threshold-free titers compared to scenarios 1 and 3. Also, since the variability of the log-ratio under scenario s=3 is either lower or comparable to that of scenario s=1, the variability of threshold-free titers under scenario 3 is lower than for scenario 1. In addition, although the

variability of the log-ratio curve under scenario 4 is higher than those of scenarios 2 and 3 at low dilutions, this curve displays non-negative killing values at all six dilutions. Therefore, the variability of its threshold free titer can be expected to be lower than that of the same titers for the other scenarios due to the larger number of dilutions available for titer estimation.

For each scenario, N=2000 threshold-based titers (2.3) were estimated using the log-ratio values simulated by (2.8) under two dose-response models: PWLI and the heteroskedastic 4PL data-generating model (2.8) estimated by maximum likelihood. Specifically, the likelihood of model (2.8) was maximized with respect to its five arguments $\alpha, \beta, \gamma, \delta$ and h using the Nelder-Mead simplex method implemented in the R routine *optim*. Threshold free titers (2.4) were estimated from the same simulations using (2.5)-(2.7) with z= 0 (T_f) and 5 ($_pT_f$) . The precision of all titers was assessed using the coefficient of variation (CV%):

$$CV_{s,k} = 100 \left(\frac{\sigma_k}{\mu_k} \right), \qquad (2.12)$$

where $CV_{s,k}$ is the value of the CV% for the *k*-th titer estimator $k = \{T_{50}^{PWLI}, T_{50}^{4PL}, T_f, _pT_f\}$ calculated for each scenario s=1,2,3,4 from the curves shown in Figure 2.2 across the 2000 simulations.

Variability of the simulation scenarios under model (8)
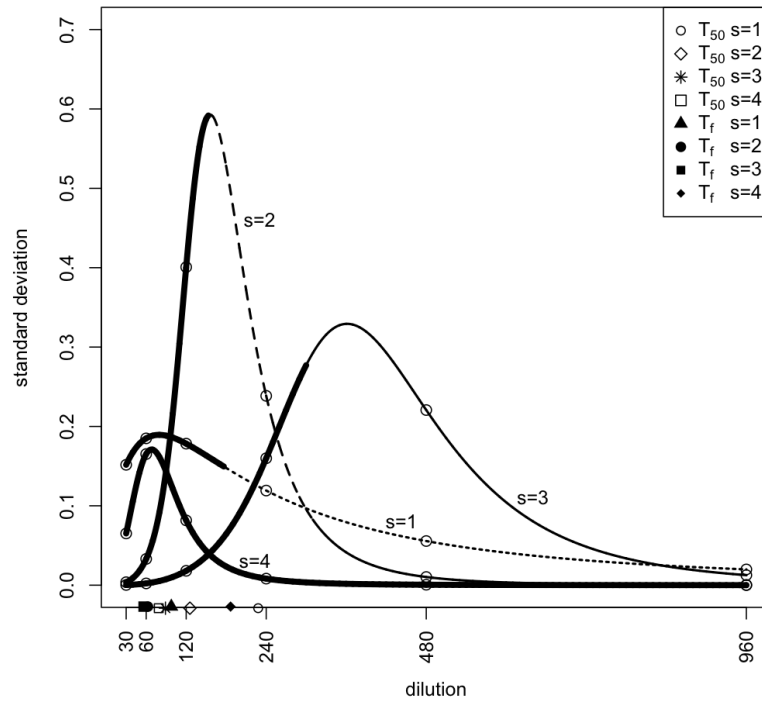
Figure 2.3: simulation variability of log-ratio-dilution curves is proportional to the first derivative of the log-ratio curve and it is more pronounced for the one left plateau point scenario (s=2).

Table 2.2 shows that the CV% of threshold-free and plateau threshold free titers was always lower (higher precision) than those of threshold-based titers using PWLI. Also, the threshold free and plateau threshold free titers (2.4) had comparable or lower CV% than threshold-based titers calculated by estimating the 4PL data-generating model. In addition, T_f are marginally more precise than $_pT_f$ due to the larger number of points used for titer estimation when $z=0$ compared to when using $z=5$. These results show that threshold-free titers were found to increase the precision of OPKA under all simulated scenarios when compared to T_{50} (PWLI) and they preserved at least the same precision of T_{50} estimated using the 4PL model.

Titer definition	Coefficient of Variation (%)			
	no plateau s=1	1 left plateau point s=2	2 left plateau points s=3	right plateau s=4
T_{50}^{4PL}	23	19	16	27
T_{50}^{PWLI}	25	22	14	26
$T_f(z=0)$	14	15	10	6
$_pT_f(z=5)$	17	21	11	12

Table 2.2: the coefficients of variation (CV%) calculated for each titer definition and data simulation scenario show that threshold-free titers tend to be more precise than threshold-based titers.

2.3.1 The precision of threshold-free titers increases in the number of serum dilutions.

Comparability of threshold-free titers across sera is ensured when all sera are tested using the same set of dilutions. Therefore, optimization of experimental design for estimating threshold-free titers requires establishing the number and value of the dilutions common to all sera. This issue is addressed here using the simulation model (2.8)-(2.11) under scenario s=3 (long left plateau) and $h = 300$. A higher value of the variance scaling h was used here compared to the simulations summarized in table 2 to measure appreciable differences across the coefficients of variation associated to different numbers of dilutions. A total of 2000 simulations were run with n= 3, 5, 9, 17 dilutions and the corresponding 2000 x 4 threshold-free titers were estimated using (2.4)-(2.5). No dilution smaller than 60 or larger than 240 was used to prevent the simulation of killing values within the plateau part of the curve or negative killing values. For, n = 3

the dilutions were [60,120,240]. Then, dilutions were equally spaced between the limits defined by each pair of dilution. For instance, for n = 5 the dilutions were [60,90,120,180,240] and so forth.

Figure 2.4 plots the CV% of the 2000 simulated threshold-free (dots) and PWLI threshold-based (asterisks) titers against the number of dilutions used in the simulations. These results show that the precision of the simulated threshold-free titers increase in the number of dilutions used for titers estimation. In particular, when 3 or 5 dilutions are used the CV% of threshold-free titers in this simulation scenario is ensured to be approximately 25% and 15% respectively. Figure 2.4 also shows that the precision of PWLI threshold-based titers does not increase with the number of dilutions. This result is due to the threshold-based titer estimates being always calculated using the *two* dilutions where killing crosses 50. Since both dilutions used for PWLI titer estimation always fall within the range of assay sensitivity the resulting CV% are invariant to the total number of dilutions used in the simulation. Based on these results, at least 3 dilutions within the OPKA sensitivity range should be used for accurate estimation of threshold-free titers from killing curves exhibiting partial saturation.

Assay precision increases with the number of dilutions
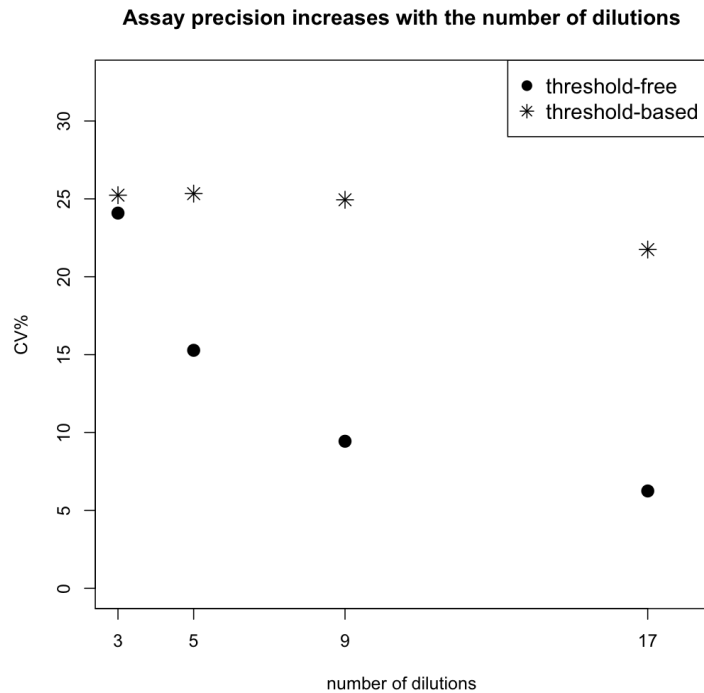
Fig 2.4: CV% of threshold-free (dots) and threshold-based (asterisks) titers calculated using different numbers of dilutions show that precision of threshold-free titers increase in the number of dilutions

2.4 Group B Streptococcus OPKA data analysis

Threshold-based and threshold-free titers were compared using repeatability and linearity experiments [29] of a research group B Streptococcus (GBS) OPKA. These experiments provide ideal data for comparing the operational characteristics of (2.3) and (2.4) because they measured a relatively large number of killing values for different sera under identical experimental conditions.

2.4.1 Estimation of OPKA titers using repeatability experiments

OPKA repeatability was measured for three of the epidemiologically dominant GBS serotypes Ia, Ib and III [1]. For each serotype, three sera were selected according to their ELISA antibody concentrations to encompass a wide range of OPKA titers. These sera are hereby referred to as serum 1 (low titer), 2 (medium titer) and 3 (high titer). The same operator assayed each serum 10 times in one analytical session using the same set of six dilutions. Table 2.3 compares the CV% of threshold-based titers using the PWLI and 4PL models and those of threshold-free titers for each serum. First, Table 3 shows that the average CV% of threshold-free titers T_f ($z=0$) across the tested sera is always the lowest among all titer definitions. This result indicates that (2.4)-(2.5) yields the most precise titer estimates among all the assessed titer estimators. Second, Table 2.3 shows that the CV% of threshold-free titers T_f are lower than those of threshold-based titers for 8/9 (one-tailed Binomial test p-value=0.02) combinations of serotype and ELISA concentration when using either PWLI or the 4PL model. This result confirms that threshold-free titers T_f tend to be more precise than threshold-based titers. The bottom three rows of each section of Table 2.3 show the CV% of the plateau threshold free titers $_pT_f$ calculated using $z = 5$, 10, 20. Overall, these CV% tend to be larger than the corresponding CV for T_f due to the lower number of dilution-killing points used for titer estimation when plateaus are excluded. Also, as an average across sera, the most precise plateau threshold free titers are obtained when using $z=20$ for serotype Ia, $z=5$ for serotype Ib and either of these two z values for serotype III.

GBS Ia OPKA titers	Coefficients of variation (CV%)			
	Serum 1	Serum 2	Serum 3	Mean
T_{50}^{4PL}	20	8	14	15
T_{50}^{PWLI}	22	8	5	12
T_f (z=0)	**6**	**12**	**2**	**7**
$_pT_f$ (z=5)	32	22	22	25
$_pT_f$ (z=10)	31	11	9	17
$_pT_f$ (z=20)	17	11	2	**10**
GBS Ib OPKA titers	**Serum 1**	**Serum 2**	**Serum 3**	**Mean**
T_{50}^{4PL}	19	25	10	18
T_{50}^{PWLI}	22	25	8	18
T_f (z=0)	**17**	**20**	**3**	**13**
$_pT_f$ (z=5)	19	30	2	**17**
$_pT_f$ (z=10)	27	26	2	18
$_pT_f$ (z=20)	36	32	18	29
GBS III OPKA titers	**Serum 1**	**Serum 2**	**Serum 3**	**Mean**
T_{50}^{4PL}	11	30	10	17
T_{50}^{PWLI}	9	17	9	12
T_f (z=0)	**7**	**14**	**3**	**8**
$_pT_f$ (z=5)	19	25	2	**15**
$_pT_f$ (z=10)	16	25	13	18
$_pT_f$ (z=20)	16	12	18	**15**

Table 2.3: CV% of threshold-free titers calculated by applying 4 different plateau conditions *z* using the GBS OPKA repeatability experiments for each combination of tested sera and serotypes

2.4.2 Estimation of OPKA titers using linearity experiments

OPKA data were generated to investigate whether titers are linear when the same serum is analysed at different starting dilutions. For each serum, linearity is assessed by plotting the starting dilutions versus their corresponding titer estimates. The experimental design used to assess OPKA linearity involved testing 4 sera for each serotype having increasing antibody concentrations as measured by ELISA (hereby referred to as sera 1 through 4). Each serum has been assayed six times (2-fold-step) in five analytical sessions using again 2-fold-step starting dilutions. For example, serum 1 for serotype Ia was assayed using the dilution sets:

$$[50,100,200,400,800,1600],$$

$$[100,200,400,800,1600,3200],$$

$$[200,400,800,1600,3200,6400],$$

$$[400,800,1600,3200,6400,12800],$$

$$[800,1600,3200,6400,12800,25600].$$

2.4.2.1 Assay linearity cannot be measured using T_{50}

To show that assay linearity cannot be measured using the threshold-based titer (2.3) it is useful to focus on the first two sets of dilutions listed above used for testing serotype Ia antibodies functionality of serum 1. For each serum, if the assay is highly repeatable the killing values associated to the common dilutions 100,200,400,800 and 1600 in the first session are the same as those measured in the second session. The same killing values will be in fact observed in any

analytical session using the same dilutions. Since T_{50} is a dilution value, it follows that using this experimental design its estimate will be the same when defined. As a consequence, when these T_{50} titer estimates are divided by the ratios of their starting dilutions to the lowest tested dilution (50/50,100/50, ... and so on) and the resulting values are plotted against these starting dilutions (50, 100, 200 and so on) in log2-log2 scale, all points will lie on a line with slope -1 by construction. This plot would further establish assay repeatability, which was demonstrated in section 4.1 above, without offering insights into the linearity of titers with respect to their starting dilutions.

2.4.2.2 Assay linearity can be measured using T_f

In contrast to what described above for T_{50} titers, T_f titers vary in their starting dilution because the right-hand side of (2.4) depends on the number and values of all dilutions used for testing and on their associated killing. Therefore, using (2.4) assay linearity becomes measureable when the assay has good repeatability.

Figures 2.5-2.7 show the log2 values of each starting dilution (horizontal axis) versus the log2 values of the corresponding estimated titers divided by the ratios of their starting dilutions to the lowest tested dilution. The plateau threshold free titer estimates depicted here were calculated using $z = 20$ for serotype Ia and $z=5$ for serotypes Ib and III. Table 2.4 shows that the threshold-free titers shown in Figures 2.5-2.7 decrease linearly in their starting dilutions with slopes of approximately -2/3 for all sera and serotypes for $z=0$ and with slopes close to -1 when the serotype-specific plateau conditions $z=5$ or $z=20$ are used. The

difference between the linearity slopes of T_f and $_pT_f$ here is imputable to the presence of left plateaus in the underlying killing curves when using lowest starting dilutions, similarly to the simulation scenario s=3 presented above.

These results show that, regardless of which plateau condition is used, threshold-free titers are measurably linear in their starting serum dilution. Also, when appropriate plateau conditions are used threshold-free titers are halved when the staring serum dilution is doubled.

Figure 2.5: Plateau threshold-free titers estimated from the GBS serotype Ia OPKA data have linearity slopes close to-1, whereas threshold-free titers slopes are close to -2/3, showing that both are linear in their starting dilution and that the plateau threshold-free titers are halved when doubling their starting dilution.

Figure 2.6: Plateau threshold-free titers estimated from the GBS serotype Ib OPKA data have linearity slopes close to -1, whereas threshold-free titers slopes are close to -2/3, showing that both are linear in their starting dilution and that the plateau threshold-free titers are halved when doubling their starting dilution.
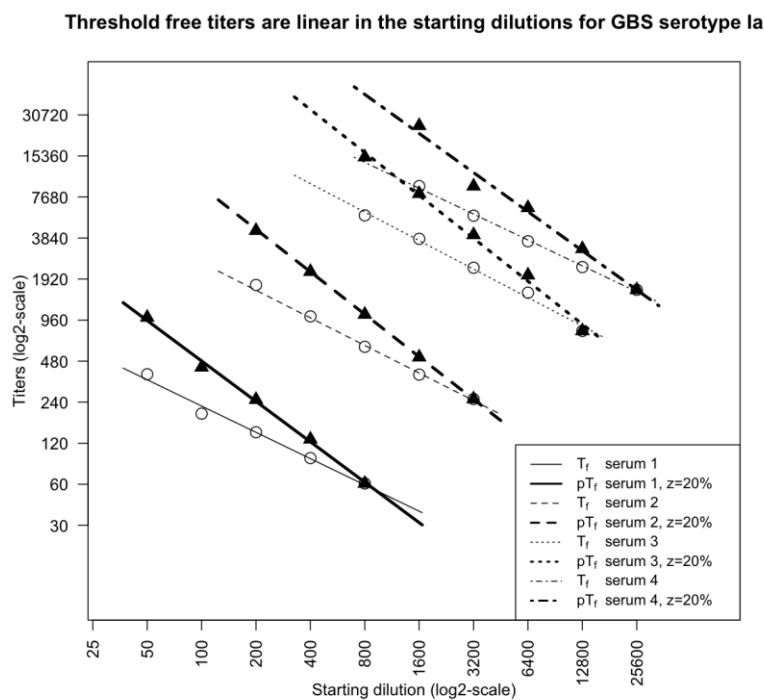

Figure 2.7: Plateau threshold-free titers estimated from the GBS serotype III OPKA data have linearity slopes close to -1, whereas threshold-free titers slopes are close to -2/3, showing that both are linear in their starting dilution and that the plateau threshold-free titers are halved when doubling their starting dilution.
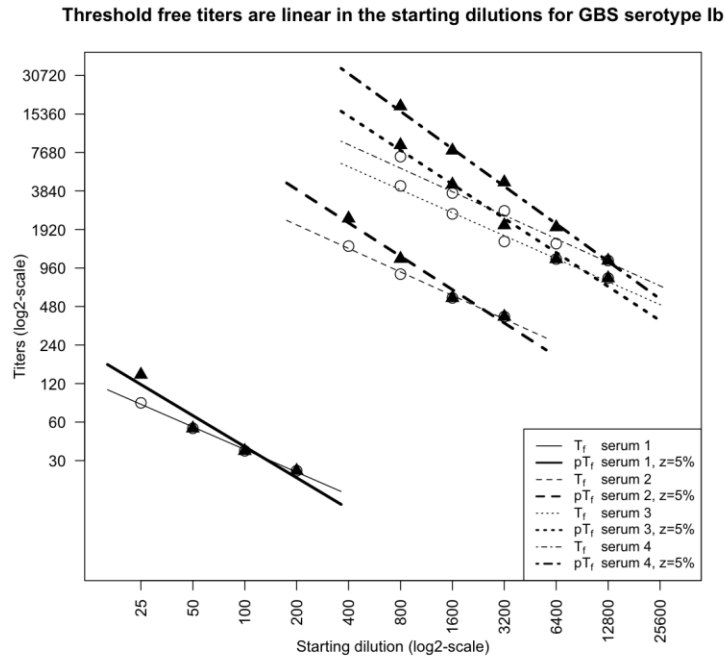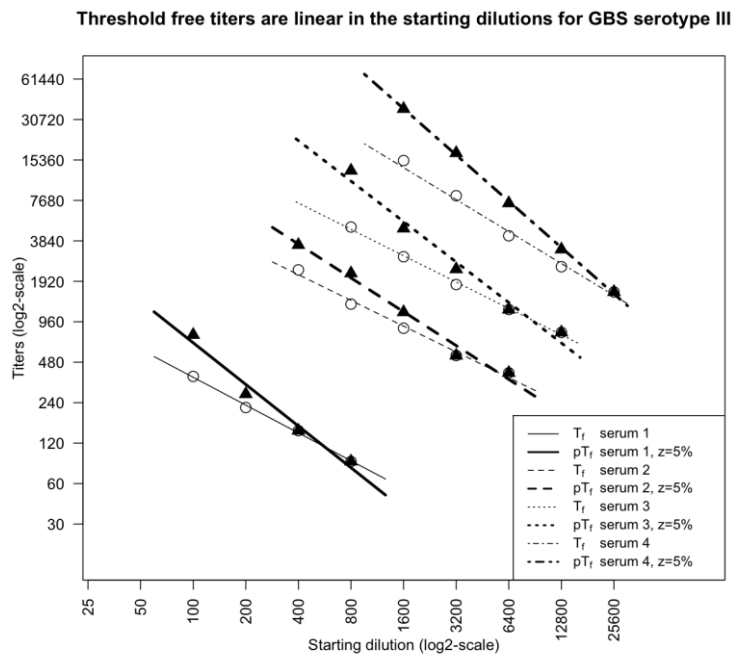
Serotype	Linearity Slopes	
	Threshold free titers **(slope and 95% c.i.)**	**Plateau threshold free titers** **(slope and 95% c.i.)**
Ia	-0.64 (-0.77, -0.51)	-0.98(-1.09, -0.87)
	-0.67(-0.77, -0.57)	-1.03(-1.05, -1.02)
	-0.69(-0.81, -0.58)	-1.05(-1.20, -0.89)
	-0.63(-0.68, -0.58)	-0.95(-1.18, -0.72)
Ib	-0.59(-0.68, -0.49)	-0.81(-1.45, -0.17)
	-0.61(-0.7, -0.45)	-0.87(-1.28, -0.46)
	-0.60(-0.72, -0.48)	-0.88(-1.09, -0.68)
	-0.61(-0.86, -0.37)	-0.97(-1.52, -0.78)
III	-0.69(-0.81, -0.57)	-1.03(-1.02, -0.53)
	-0.63(-0.76, -0.51)	-0.83(-1.28, -0.65)
	-0.65(-0.72, -0.59)	-1.00(-1.27, -0.72)
	-0.79(-1.04, -0.54)	-1.14(-1.27, -1.02)

Table 2.4: the linearity regression slopes and their asymptotic Gaussian confidence intervals show that plateau threshold-free titers are halved when their starting dilution is doubled.

2.5 Summary and discussion of Chapter 2

The biological interpretability of threshold-free titers as weighted averages of tested serum dilutions, their higher precision compared to threshold-based titers and the measurability of titer linearity demonstrated in this paper indicate that threshold-free titers (2.4) are appropriate tools for analysing OPKA data.

Unlike for threshold-based titers, experimental designs for estimating biologically relevant and accurate threshold-free titers require testing different sera using the same set of dilutions. This set of serum dilutions can be determined by setting three design parameters: the extreme (minimum and maximum) killing values to be measured and the lowest number of dilutions associated to non-negative killing values for all sera. For instance, the maximum killing may be required to exceed 50 and the minimum killing may be required to be less than zero, showing bacterial proliferation. The simulation study presented in this paper shows that precise threshold-free titers can be estimated using as few as three dilutions associated to non-negative killings.

Assay saturation is taken into account in this paper using a plateau condition determined prior to estimation of threshold free titers. From this angle, a threshold-free titer estimator that automatically down-weights the dilutions associated to saturated killing would be desirable. This can be achieved by making the weights (2.5) functions of the slope of the log-ratio curve with respect to dilution. The construction of such weights requires a continuous dose response model and robust computational routines for titer estimation. The simulation model (2.8) used in this paper is a first step in this direction using a standard 4PL mean structure and a dilution-dependent variance function.

Estimation of threshold-free titers under this model requires extending their definition to the continuous case as an integral and adopting robust numerical techniques such as Monte Carlo importance sampling [30]. The assessment of whether such model-based titer estimates could become part of the routine analysis of OPKA data is a topic currently under investigation.

CHAPTER 3 Bayesian modeling of functional antibody titers[3]

Chapter 2 of this thesis illustrated a novel definition of antibody titers that is based neither on a bacterial killing threshold nor on the selection of a dilution-killing model. This definition was generalized to take into account the potential biasing effects of assay saturation either above or below (plateaus), consisting of a user-defined additional parameter $z \in (0,100)$ within the definition of the weights (formulas 2.6-2.7). This *plateau condition* specifies the smallest biologically interpretable jump in the dilution-killing curve. Compared to threshold-free titers using $z = 0$, plateau threshold-free titers were shown to be less precise due to the less number of point used for titer calculation, but they do preserve better precision compared to T_{50}. However, the choice of an optimal plateau condition for each of the analysed sera remains unaddressed by this simple approach, because the value of z is based on general biological considerations as opposed to being tailored to the dose-response measured for each serum using statistical methods. These methods would thus rely on an estimation process having the goal to maximize the precision of the resulting procedure for each serum. To fully address this issue in this Chapter a threshold-free titer definition that automatically takes into account the occurrence of plateau is proposed and investigated. Following an established tradition of bioassay data modeling and analysis [30-34], this new proposal is developed within a Bayesian approach to dose-response modelling and relies both on the dilution-dependent slope of a smooth dilution-killing model for down-weighting

---

[3] Chapter 3 adapted from: "Bayesian Modelling of functional antibody titers". L.Moraschini, M.Fabbrini, I.Margarit Y Ros, F.Rigat. Submitted for publication.

points associated to its plateau regions and on the selection of a set of prior distributions for the coefficients of the dilution-killing model. These priors summarize the maximum likelihood regression estimates of the dilution-killing curves measured in replicate experiments performed during assay characterization (data shown in Chapter 2).

The properties of this new method will be first assessed using a simulation analysis similar to that shown in Chapter 2, using different number of scenarios and different ranges of dilutions; then the operational characteristics of this new method will be assessed using data from the European study DEVANI [42] that has the goal to develop immunization strategies for inducing immunity against GBS.

3.1 Integrated titers definition

A threshold free model based generalization of (2.4) using continuous weights that automatically take into account the saturation of each analysed killing curve while preserving biological interpretability is the Integrated titer:

$$T_I = \frac{\int_{d_m(\underline{\theta}_i)}^{d_M(\underline{\theta}_i)} x k(x|\underline{\theta}_i) |dk(x|\underline{\theta}_i)|}{\int_{d_m(\underline{\theta}_i)}^{d_M(\underline{\theta}_i)} k(x|\underline{\theta}_i)|dk(x|\underline{\theta}_i)|} \,. \tag{3.1}$$

In (3.1) the function $k(x|\underline{\theta}_i)$ represents a continuous dose-response model with sample specific coefficients θ_i.

Integrated titers (3.1) average all dilutions within the range $(d_m(\underline{\theta}_i), d_M(\underline{\theta}_i))$ with respect to an assumed dilution-killing model $k(x|\underline{\theta}_i)$ multiplied by its first

derivative. Using the first derivative Integrates titers automatically estimates antibody functionality from the unsaturated region of the dilution-killing curve. According to what considered for threshold free titers (2.4) the range $(d_m(\underline{\theta}_i),$ $d_M(\underline{\theta}_i))$ is defined as follows:

$$d_m(\underline{\theta}_i) = \min_{x \in [d_1, d_J]}\left\{k\left(x\middle|\underline{\theta}_{i_i}\right) \geq 50\right\}, \qquad (3.2)$$

$$d_M(\underline{\theta}_i) = \max_{x \in [d_1, d_J]}\left\{k\left(x\middle|\underline{\theta}_i\right) \geq 0\right\}.$$

The interpretation of Integrated titers (3.1) is analogous to that of threshold free titers: it is the mean of the dilution weighted for the corresponding killing values and the first derivative values. In other words, Integrated titers quantify the antibodies functionality from the *unsaturated* part of the dilution-killing curve.

In addition, Integrated titers preserve all properties of threshold free titers listed in table 2.1 (uniqueness, threshold-independence and use of all data points). Also, Integrated titers depend on the set of assumptions built into the dilution-killing model required for estimation of (3.1).

When the killing curve is linear within the dilution range $(d_m(\underline{\theta}_i),$ $d_M(\underline{\theta}_i))$, both titer estimators T_I and T_{50} have closed forms.

In this case, necessary and sufficient conditions for equality of titers can be derived explicitly. We present these results in the following theorem.

Theorem 3.1 *Let $\tau \in (0,100)$ be the critical killing threshold used in (2.3) and let $k(d|\alpha,\beta) \approx \alpha + \beta d$ within the dilution range $d \in \left[d_1, -\frac{\alpha}{\beta}\right]$ with $d_1 > 0, \beta < 0$ and $\alpha + \beta d_1 \geq \tau$. Then, the followings hold:*

I. $T_\tau(\alpha, \beta) = \frac{\tau - \alpha}{\beta}$,

II. $T_I(\alpha, \beta) = \frac{-(\alpha^2 - \alpha\beta d_1 - 2\beta^2 d_1^2)}{3\alpha\beta + 3\alpha\beta^2 d_1}$

Proof. For any given τ the value of the threshold-based titer T_τ in the first statement I trivially follows from inversion of the linear killing curve.

To demonstrate statement II, let the killing curve be linear within the generic range (X_L, X_U) and plug the expression of the linear killing curve in (3.1) so that:

$$T_I(\alpha, \beta) = \frac{\int_{X_L}^{X_U} x(\alpha + \beta x)dx}{\int_{X_L}^{X_U} (\alpha + \beta x)dx}$$

$$= \frac{\frac{\alpha}{2}(X_U^2 - X_L^2) + \frac{\beta}{3}(X_U^3 - X_L^3)}{\alpha(X_U - X_L) + \frac{\beta}{2}(X_U^2 - X_L^2)}$$

$$= \frac{\alpha(X_U + X_L) + \frac{\beta}{3}(X_U^2 + X_L X_U + X_L^2)}{\alpha + \frac{\beta}{2}(X_U + X_L)}$$

Statement II follows by substituting $X_L = d_1$ and $X_U = -\frac{\alpha}{\beta}$ in the right-hand side of the above equation.

Lemma 3.1 Under the conditions of Theorem 3.1 for any given (τ, α, d_1) T_{50} and T_I yield the same titer value iff there exist at least one value $\beta^* < 0$ such that

$$\beta^* = \frac{3d_1\tau - 4\alpha d_1 \pm \sqrt{(-3d_1\tau + 4\alpha d_1)^2 - 8d_1^2(2\alpha^2 - 3\alpha\tau)}}{4d_1^2} \qquad (3.3)$$

Lemma 3.1 shows that, having fixed by design the initial dilution d_1 and the critical killing threshold τ, for any intercept α there may exist up to two slope values such that T_{50} and T_I coincide. Here we present a numerical example deriving the values of the killing slope yielding equality of Integrated titers and threshold baser titers.

Example 3.1 *For α = 100, τ = 50 and d_1=30 two distinct killing slopes β^* exist, with values then -0.83 and -3.33. Since only the value -0.83 fulfils the conditions of theorem 3.1, in this case there exists a unique linear killing functions ensuring equality of T_{50} and T_I. For values of β respectively larger (smaller) than -0.83 the threshold based titer $T_{50}(100, \beta)$ becomes larger(smaller) than $T_I(100, \beta)$*

Example 3.1 implies that, when doubling a serum dilution halves the bacterial killing, $T_{50}(100, -1)$ =50. In this case, $T_I(100, -1)$< $T_{50}(100, -1)$ for d $\in$ (0,25) and $T_I(100, -1)$>$T_{50}(100, -1)$ for d $\in$ (25,50) with d_1=25 yielding equality of titers. This example demonstrates that values of T_{50} estimated from experimental data would be in general more sensitive to the range of tested dilutions fixed a priori by design compared to T_I. Titer estimation will be illustrated in detail in the next section.

3.2 Model based estimation of Integrated titers

In Chapter 2 a likelihood free approach was used to estimate both threshold free titers and T_{50} titers. In this Chapter a likelihood-based approach is used both for the estimation of Integrated titer and T_{50} titers.

Accordingly to what shown in the first Chapter, the log-ratio likelihood was used for each serum i at dilution d as follows:

$$LR_{id} \sim N(\mu(d_i|\underline{\theta}_i), h_i * \mu'(d|\underline{\theta}_i)), \tag{3.4}$$

where $\mu'(d_i|\underline{\theta}_i) = \dfrac{\partial\,\mu(d_i|\underline{\theta}_i)}{\partial d}$

the mean structure of model (3.4) needs to incorporate the features of bioassay data: the occurrence of finite upper and lower asymptotes and a monotone relation between dilution and log-ratio. To incorporate this constraint the 4PL logistic model was used as in Chapter 2:

$$\mu\left(d, \underline{\theta}_i\right) = \delta_i + \frac{\alpha_i - \delta_i}{1+\left(\frac{d}{\gamma_i}\right)^{\beta_i}} \text{ so that } \underline{\theta}_i = [\alpha_i, \beta_i, \gamma_i, \delta_i] \tag{3.5}$$

The variance of model (3.4) reflects another typical feature of bioassay data, defining proportionality between assay saturation and precision of the measured log-ratio data up to an unknown and possibly serum-dependent coefficient h_i. Under (3.6) and taking the log-ratio data as conditionally independent given the

model coefficient $\underline{\theta}_i$ and the tested dilution $(d_1,...,d_J)$ the log-likelihood of the log-ratio data is:

$$l(LR_{i1},\ldots,LR_{iJ}|\underline{\theta}_i,d_1,\ldots,d_J) \propto -\frac{1}{2h_i}\sum_{j=1}^{J}\left(\frac{LR_{ij}-\mu(d_j,\underline{\theta}_i)}{\mu'(d_j,\underline{\theta}_i)}\right) \qquad (3.6)$$

3.2.1 Measurement error priors

Identifiability of $\underline{\theta}_i$ under (3.4) even when J>5 is problematic due to $\mu(d_j,\underline{\theta}_i)$ being invariant to simultaneous inversion of the signs of $(\alpha_i,\delta_i,\beta_i)$ at any dilution d.

as $\alpha_i>\delta_i$, or by fixing a priori the sign of the slope coefficient β_i [35]. Here we take a different approach, by defining the prior probability distribution for each component of $\underline{\theta}_i$ independently by modelling the frequency distribution of the maximum likelihood estimates (MLEs) of each model parameter. These MLEs were calculated from the set of OPKA experiments used in Chapter 2.4.1 for the repeatability analysis, which are experiments run under the same identical condition for each of the 9 sera tested. Only sera where maximum killing exceeded 50 and the minimum estimated killing was larger than the theoretical maximum bacterial proliferation within the assay time (-300) were considered for the prior specification. Therefore, as opposed to representing an a priori subjective opinion of the experimental scientist, these priors quantify the expected range and variability of the model parameters induced by the experimental error measured when testing in OPKA a wide range of human sera.

Figure 3.1 shows the kernel density estimates for the distributions of $(\alpha_i, \beta_i, log(\gamma_i), \delta_i, \log(h_i))$. All five distributions seem symmetric and amenable to be tested for the hypothesis of Gaussian distribution.

The p-values of the Kolmogorov-Smirnov statistics testing Gaussianity of the MLE frequency distributions of $(\alpha_i, \beta_i, log(\gamma_i), \delta_i, \log(h_i))$ were (0.17, 0.36, 0.32, 0.10, 0.28) respectively. Since none of these p-values indicated a gross inconsistency between the observed MLE frequencies and the Gaussian distribution, the prior distributions used here were

$$\alpha_i \sim N(1.4, 0.8) \qquad\qquad (3.7)$$

$$\beta_i \sim N(-2.4, 1.3)$$

$$\delta_i \sim N(-4.7, 1)$$

$$\gamma_i \sim LN(7.4, 1.4)$$

$$h_i \sim LN(4.2, 0.5)$$

where N(a,b) and LN(a,b) indicate respectively the Gaussian and log-Normal distributions with mean equal to a and SD equal to b. The prior moments in (3.7) matched the empirical moments of each parameter's MLEs. Consistently to what presented in Chapter 2, in this section threshold based titers T_{50} will be calculated using the dilution-logratio model (3.5) to interpolate dilution-logratio data points.

Figure 3.2 depicts the prior predictive mean and the point-wise prior predictive intervals for the killing curve (left panel) and the prior predictive distributions of the threshold-based T_{50} and Integrated titers under (3.6) and (3.7). The prior predictive killing mean (whole black curve in Figure 3.2) displays a visible

saturation to the left, corresponding to dilution factors lower than 1000 and to very high killing values, reflecting the relatively high concentrations of functional antibody in the sera used for defining this prior. Also, the prior predictive intervals around the mean are very wide, suggesting that the strength of this prior is low. Despite the substantial difference between the titer functionals T_{50} and T_l the right panel in Figure 3.2 shows that their prior distributions are very similar, being approximately symmetrical in the log-dilution factor with interquartile range of approximately (670, 4500) and prior predictive mean of 2900. Figure 3.2 implies that a priori neither of the two titer definitions is expected to yield appreciably different point estimates or titer estimates with different precision.
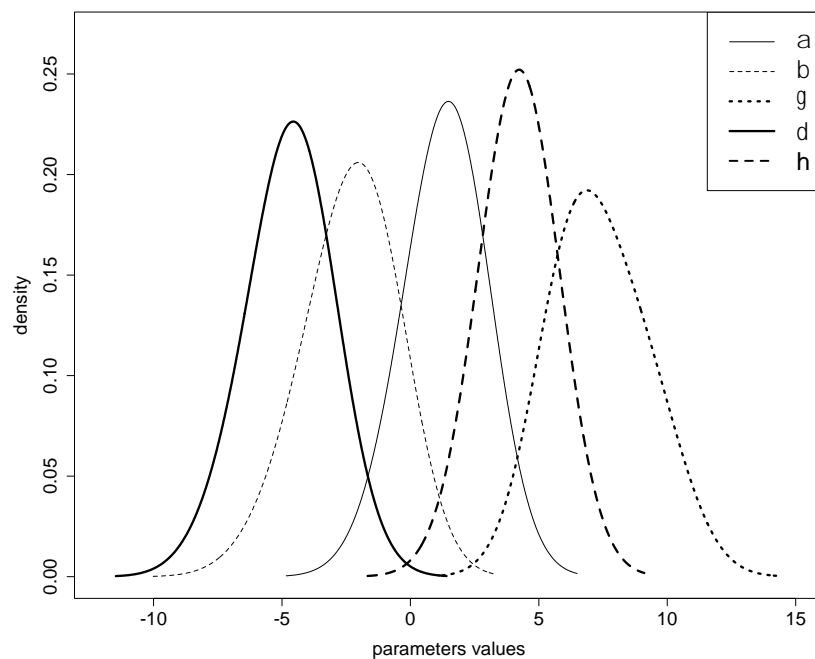

Figure 3.1: kernel density estimate for the distributions of ($\alpha_i, \beta_i, log(\gamma_i), \delta_i, log(h_i)$). All five distributions seem symmetric and amenable to be tested for the hypothesis of Gaussian distribution. The Kolmogorov-Smirnov P-Values (0.17, 0.36, 0.32, 0.10, 0.28) indicate that this hypothesis can't be rejected
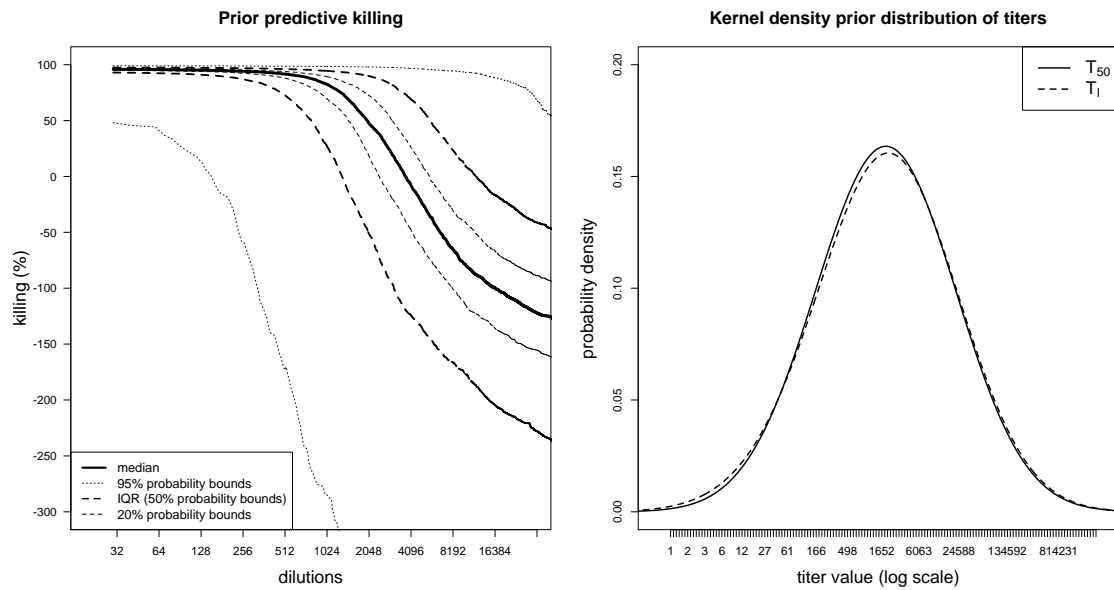
Figure 3.2: the left panel shows the prior predictive dilution-killing mean (whole curve) along with its 95%, 50% and 20% prior probability intervals. The right panel shows the prior predictive distributions of T_{50} and T_I titers. These distributions are closely matched, being approximately symmetrical in the log-dilution factor with interquartile range of approximately (670, 4500) and prior predictive mean of 2900.

3.2.2 Posterior inference

Under the likelihood (3.6) and priors (3.7), the conditional posterior distributions of the coefficients $\underline{\theta_i}$ are not closed under sampling, so that marginal posterior estimates need begin approximated using numerical techniques. To this end, an independent sampler Markov chain Monte Carlo (MCMC) was used with proposal distributions for each of the coefficients $(\alpha_i, \beta_i, \gamma_i, \delta_i, h_i)$ centred at their maximum likelihood estimates (MLEs) and with standard deviations (0.1,0.1,0.1,0.05,0.05). These proposals yielded mixing rates approximately matching the optimal 0.234 [36] with one proposed value being

accepted every three to six iterations. Each of the two titers T_{50} and T_I were calculated at each iteration of the MCMC and approximate marginal posterior median titers were estimated using ten thousand iterations. Given the model parameters, calculation of the threshold-based titer T_{50} is analytical [28], whereas no closed-form expression for the integrated titer T_I is available. The integral defining (3.2) was then approximated numerically within the MCMC by using importance sampling with a uniform importance density over the range of dilutions yielding non-negative killing values.

3.3 Operational characteristics of threshold free Integrated titers using simulated data

OPKA curves were simulated using the likelihood (3.6) under the three scenarios shown in Figure 3.3. In this figure, the curves are represented first on the dilution-Logratio scale (left panel) and then on the dilution-killing scale (right panel). These scenarios respectively represent pronounced assay saturation at low dilutions (s=1 or "left plateau"), no assay saturation (s=2 or "no plateaus") and pronounced assay saturation at high dilutions associated to non-negative killing values (s=3 or "right plateau"). Table 3.1 shows the values of the model parameters associated to these three scenarios used to calculate the Logratio killing curves, as well as the corresponding values of T_{50} and T_I titers and the values of the variance scaling factors h used to simulate OPKA data around these expected OPKA curves. A lower h value was used when simulating from the no plateaus scenario, because the derivative of the log-ratio curve is large and constant over the range of dilutions. This value was used to generate OPKA data

using standard deviations comparable to those used when simulating from the other two scenarios where the first derivative is less pronounced. As shown in Table 3.1, the left plateau curve displays the maximum associated titer, irrespectively of whether T_{50} or T_I are used. Titer T_{50} for the no plateaus scenario (s=2) is larger than that of the same titer for the right plateau curve (s=3) whereas the opposite is true for titers T_I. This difference is due to the insensitivity of T_{50} to the long tail of positive killing values of the right plateau scenario. Since this curve has non-negligible first derivative within the dilution interval (0,10000), titer T_I is pulled to the right compared to its value for the no plateaus curve. These numerical discrepancies reflect the inherent difference in the notions of antibody functionality embedded in the titer definitions T_{50} and T_I, in that T_{50} reflects the dilution associated to one killing value whereas T_I summarizes the pattern of the OPKA curve over the range of assay sensitivity.
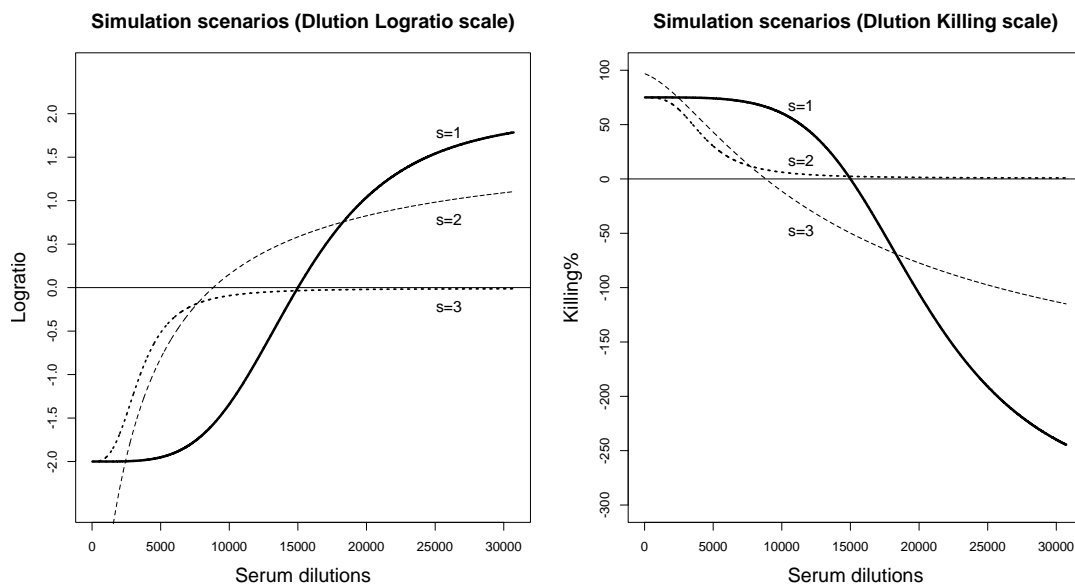

Figure 3.3: dilution-logratio (left panel) and corresponding dilution-killing (right panel) sigmoidal curves for three illustrative scenarios, displaying a pronounced saturation at low dilutions (s=1 or ``left plateau''), no saturation (s=2 or ``no plateaus'') and a pronounced saturation at high dilutions associated to non-negative killing values (s=3 or ``right plateau''

Serotype	lef plateau	no plateaus	right plateau
α	-2	-5	-2
β	4	1	3
γ	15000	3000	3500
δ	2	1.7	-0.012
T_{50}	11397.5	4444.4	3511.7
T_I	10687.1	3215.7	3566.8
H	30000	300	10000

Table 3.1: values of the model parameters (3.6) defining the three simulation scenarios depicted in Figure 3.3 corresponding titers T_{50} and T_I and corresponding variance scaling factors h used to simulate data

Figure 3.4 shows the simulation results with N=2000 for each of the three simulated scenarios. The dilution values used here were (30, 120, 480, 1920, 7680, 30720), closely mimicking the assay characterization experiments used to derive the prior predictive distributions shown in Figure 3.2. Each point displayed in the upper panels of Figure 3.4 plots one estimated titer T_{50} versus its corresponding titer estimate using T_I. The lower panels of Figure 3.4 plot the coefficients of variation (CV%) of each titer estimate (T_{50}) calculated along its Markov chain versus the CV% of the corresponding titer estimate T_I.

The upper left panel in Figure 3.4 shows that a tight linear relationship was observed between the estimated titers T_{50} and T_I for the left plateau scenario (Pearson correlation coefficient >99 and slope equal to 0.92), with integrated

titer estimates taking lower values than the corresponding threshold-based titers in the upper range consistently with the true titer values displayed in Table 3.1. Also, the lower left panel in Figure 3.4 shows that both titer estimates are equally precise, with maximum CV% lower than 6%. The upper central plot in Figure 3.4 shows that the linear relationship between the titer estimates T_{50} and T_I is also very strong for the no plateau scenario (Pearson correlation = 0.95 and slope equal to 0.63) but the Integrated titer estimates are consistently smaller than their corresponding threshold-based titer estimates. This result can be explained by noting from Figure 3.3 that the positive portion of the killing curve of this simulation scenario is approximately linear, with slope larger than its critical value β^*.

The lower central panel in Figure 3.4 shows that the CV% of the integrated titer estimates for this simulation scenario tend to be lower than the CV% of the corresponding threshold-based estimates, demonstrating that T_I provides a more precise quantification of antibody functionality in absence of assay saturation. The upper right panel in Figure 3.4 shows that integrated titer estimates for the right plateau simulation scenario tend to be larger than the corresponding threshold-based titer estimates, preserving excellent linearity (Pearson correlation=0.96 and slope equal to 1.02). Consistently with the true titer values shown in Table 3.1, this discrepancy is due to the ability of T_I to reflect the positive killing values at high dilutions over portion of the OPKA curve having non-negligible first derivative. The lower right panel in Figure 3.4 shows that also for this scenario the CV% of the integrated titer estimates tend to be much lower than the CV% calculated on the corresponding threshold-based estimates, again providing a more precise measure of antibody functionality. In

general, the results of the simulation analysis indicate that Integrated titers are linearly related to traditional T_{50} titers, and they are more precise in terms of coefficient of variation calculated on each single simulated serum. This result is a first good indication because the scenarios considered in this analysis are representative of the routinely analysed serum samples of OPKA dilution-killing data.
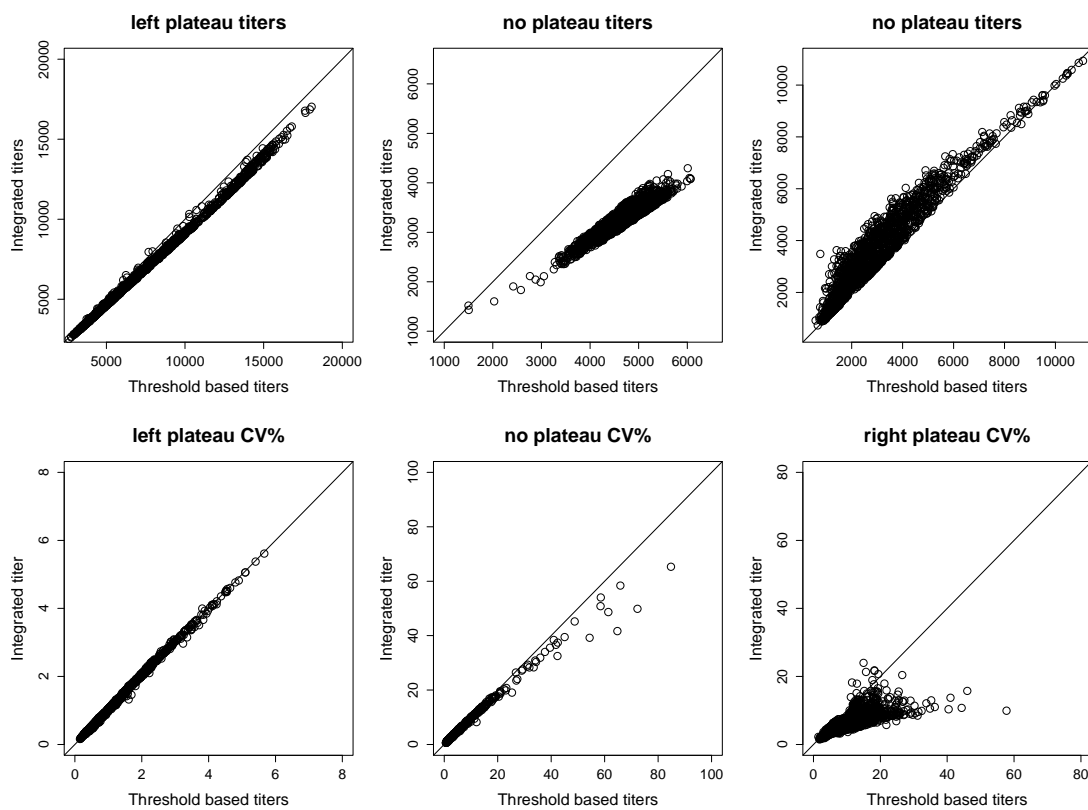
Figure 3.4: each point displayed in the upper panels plots one titer T_{50} estimated from simulated data versus its corresponding titer estimate using T_I. The lower panels plot the coefficients of variation (CV%) of each titer estimate T_{50} calculated along its Markov chain versus the CV% of the corresponding titer estimate T_I. Strong linear relationships between the two titer estimates are observed for all simulation scenarios. The CV% associated to both titer definitions estimated from the left plateau scenario are consistently low. The CV% of the Integrated titers for the other two scenarios tend to be lower than those of the threshold-based titer estimates, indicating that in these cases T_I provides a more precise quantification of antibody functionality

3.4 Operational characteristics of threshold free Integrated titers using DEVANI data

Functional antibody titers were estimated using T_{50} and T_I from a set of OPKA experiments performed on human sera collected in the context of the DEVANI study (www.devaniproject.org). The aim of this study was to characterise the seroepidemiology of group B Streptococcus (GBS) in pregnant women in Europe. The data analyzed here were collected from 30, 43, 53 randomly selected human sera respectively for the three GBS serotypes Ia, Ib, III. Unlike in the simulation example illustrated above, each serum analyzed here was tested using 4 serum dilutions, comprised between a minimum of 30 and maximum of 10800. Therefore, unique maximum likelihood estimates of the five coefficients of model (3.5) are not possible from this limited number of data. In this case, the Bayesian approach offers two big advantages: first the titer estimation leverages the assay characterization experiments via the priors (3.7) incorporating the key knowledge that these experiments has offered; second it also makes possible and meaningful the estimation of a unique titer for each analysed serum.

Independent MCMC runs with length 2000 iterations were used when estimating T_{50} and T_I for different sera, yielding acceptance rates within 10% and 40%.

The upper panels of Figure 3.5 show the posterior median estimates of T_{50} (horizontal axis) plotted against those of T_I for each analysed serum and for each of the three GBS serotypes. The two titer point estimates are very similar, with the T_I titers displaying marginally lower values than the corresponding T_{50} estimates consistently with the simulation results displayed in Figure 3.4. Similar results were obtained when using the posterior mean as titer point estimate. The lower panels in Figure 3.5 show the relationship between the posterior CVs of

each T_{50} and T_I titer estimate analogously to Figure 3.5. For serotype Ia (left panel), the proportion of CV% of T_I titers lower than those of the corresponding T_{50} estimates is 22/30 = 73%. For serotype Ib, 29/43 =67% of T_I CV% are lower than those of the corresponding T_{50} estimates. For serotype III (right panel), 40/53= 0.75% of T_I CV% are lower than those of T_{50} titers. These results indicate that T_I titer estimates are more precise than T_{50} estimates (Binomial test p-values < 0.05 for all three serotypes), although this difference is less pronounced than for simulated data due for instance to the lower range of CV% values estimated from experimental OPKA data.
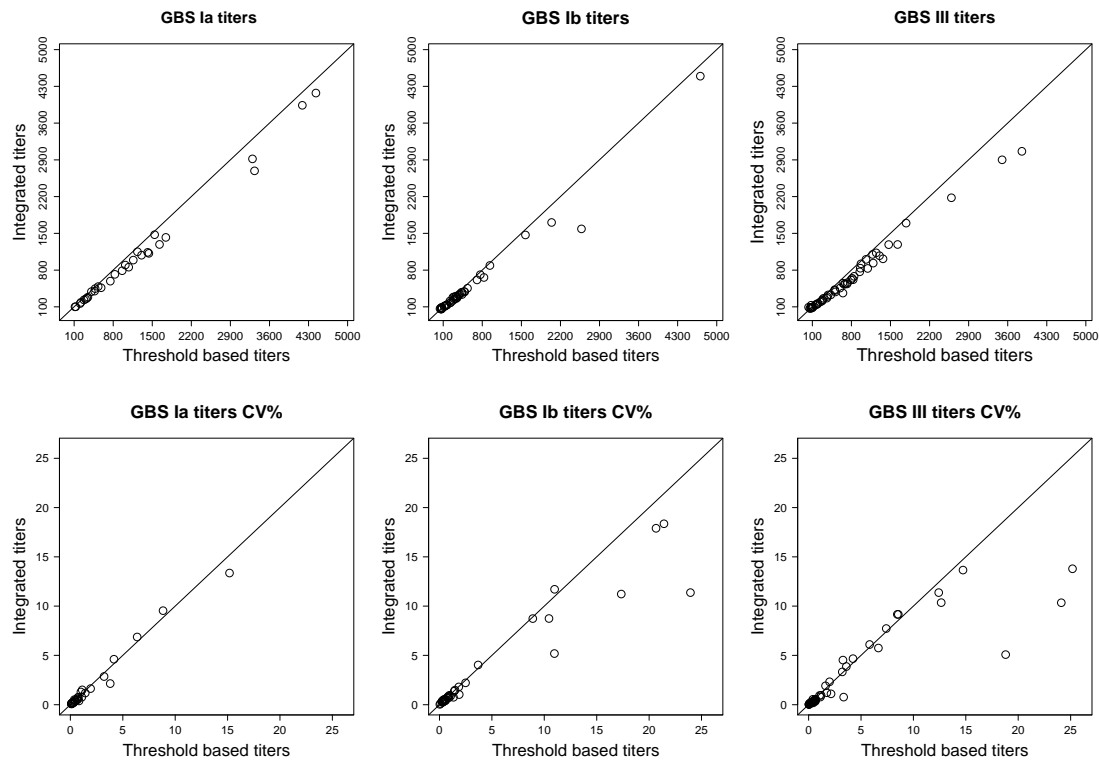
Figure 3.5: posterior median estimates of T_{50} (horizontal axis) plotted against those of T_I for each analyzed serum and for each of the three GBS serotypes (upper panels). The relation between the two point estimates is linear, as in the simulation results shown in Figure 3.4, with T_I titers displaying marginally lower values than the corresponding T_{50} estimates. The lower panels show the relation between the posterior CVs of the T_I and T_{50} titer estimates analogously to Figure 3.4. The CVs of T_I estimates are consistently lower than those of the corresponding T_{50} estimates, indicating again that T_I titers provide more precise quantifications of antibody functionality compared to T_{50} titers

The upper-left panel in Figure 3.6 shows the dilution-killing data, estimated posterior killing and titers for one serum tested in OPKA for serotype III GBS antibody functionality. In this case the posterior medians of T_I and T_{50} almost coincide, taking values 72 and 73 respectively. The upper-right panel in Figure 3.7 compares the positive portion of this estimated killing curve to the linear interpolant passing through the two measured dilution-killing data points, with coordinates (30,76) and (90,39). Since the linear interpolant closely resembles the estimated killing curve, Theorem 3.1 and Lemma 3.1 apply in this case. The linear interpolant has intercept $\alpha = 94.5$ and slope $\beta = -0.62$. Since $d_1 = 30$ here, using Lemma 3.1 with $\tau = 50$ and $\alpha = 94.5$ the slope value ensuring equality of titers is $\beta^* = -0.65$. The proximity between the estimated killing curve under (3.6) and (3.7) to the linear interpolant combined with the small discrepancy between β and β^* explain why in this case the T_I and T_{50} estimates are very close both to each other and to the titer estimates calculated from the linear interpolant using Theorem 3.1 (taking respectively values 71 and 72).

The lower panels in Figure 3.7 show the data and killing curves for two additional sera. The left panel shows one case where $\hat{T}_{50} = 33$ and $\hat{T}_I = 93$, so that $\hat{T}_{50} < \hat{T}_I$. These titer estimates represent a killing curve barely exceeding 50 at the lowest dilution and having moderate slope. The right panel illustrates the killing curve of a different serum, where $\hat{T}_{50} = 1365$ and $\hat{T}_I = 1015$. Here the killing associated to the lowest dilution is close to 100 and most of the non-negative killings are associated to dilutions lower than $\hat{T}_{50}$ so that $\hat{T}_{50} > \hat{T}_I$. In both cases $\hat{T}_{50}$ fails to represent most of the killing pattern, being by construction independent of the killing values observed respectively at higher or lower dilutions. In

contrast, $\hat{T}_I$ more closely reflect the killing curves of these human sera, which exhibit many non-negative killing values respectively above and below $\hat{T}_{50}$.
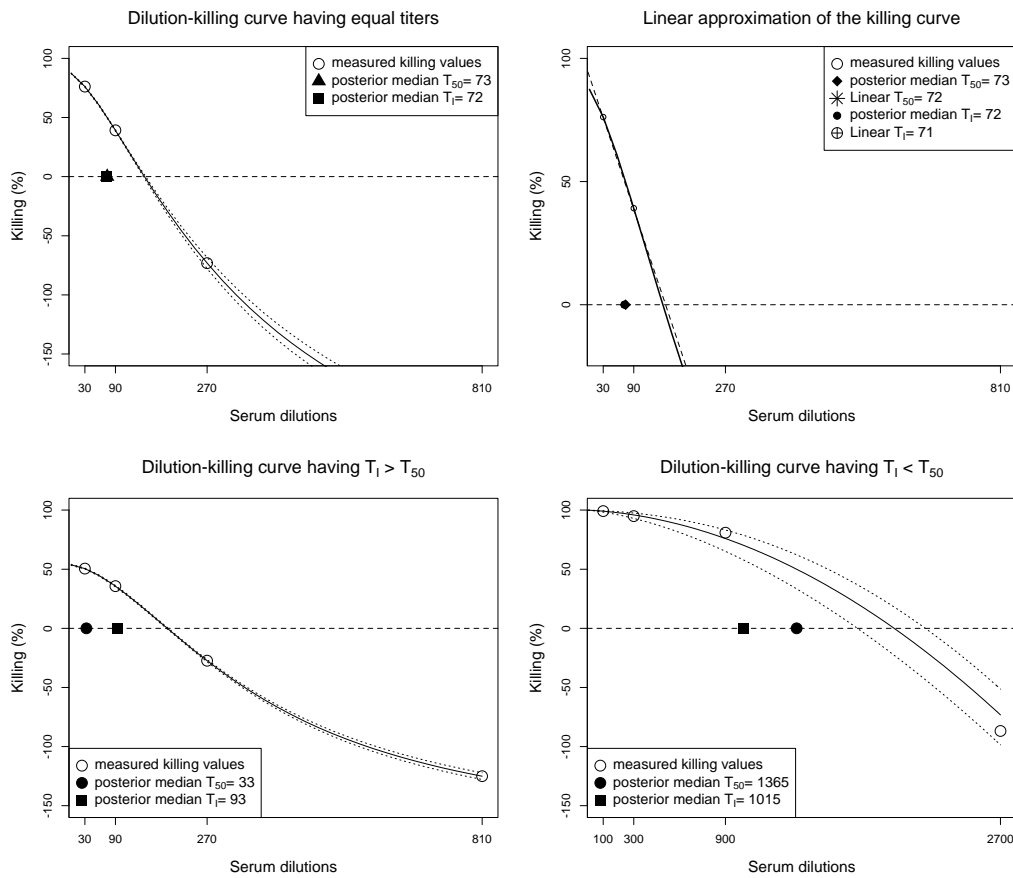

Figure 3.6: dilution-killing data, estimated posterior killing and titers for one serum tested in OPKA for serotype III GBS (upper left panel). Since the linear interpolant closely resembles the estimated killing curve, Theorem 3.1 and Lemma 3.1 apply in this case (upper right panel). The proximity between the killing estimated under (2.6) and (2.7) to the linear interpolant and the small difference between $\beta = -0.62$ and $\beta^* = -0.65$ explain why in this case the T_I and T_{50} estimates are very close to each other (72 and 73) and to the titer estimates calculated from the linear interpolant (71 and 72). The lower panels show the killing curves of two other sera where $\hat{T}_{50} = 33$ and $\hat{T}_I = 93$ (left panel), so that $\hat{T}_{50} < \hat{T}_I$, and $\hat{T}_{50} = 1365$ and $\hat{T}_I = 1015$. (right panel), so that $\hat{T}_{50} > \hat{T}_I$. In both cases $\hat{T}_{50}$ fails to reflect most of the killing curve, whereas $\hat{T}_I$ more closely reflect the many non-negative killing values respectively above and below $\hat{T}_{50}$

3.5 Summary and discussion of Chapter 3

Here the threshold-free titer definition proposed in Chapter 2 was extended so as to incorporate an assumption of monotonicity of the dilution-killing curve, as reflected by the 4PL model. The main strength of this approach is that saturation of the killing curve is automatically taken into account when estimating threshold-free titers, as opposed to being accounted for by specification of the plateau condition z. In this way the plateau occurrence is handled from a statistical point of view that automatically incorporate the biological meaning (down-weight of plateau).

In addition, this Chapter demonstrates three main strengths of a Bayesian approach to modelling and analysis of antibody functional activity. First, prior distributions derived from assay characterization experiments establish a formal link between the assay operational characteristics and the analysis of subsequent data. Second, these priors robustify titer estimation when the number of tested dilutions is low. Third, marginal posterior distributions provide estimates of titer precision without relying on the asymptotics underpinning the derivation of confidence intervals.

This work thus poses the bases for Integrated titers to become a tool for the analysis of clinical data. In practice, this will be possible if the numerical methods for titer estimation are implemented efficiently for routine use.

For instance, the Markov chain Monte Carlo sampler used here does not exploit the posterior conjugacy of the variance scaling coefficient h, which would ensue from using an Inverse Gamma prior. If this prior can be supported by further assay characterization experiments, then h can be integrated out of the joint

posterior thus simplifying the posterior sampling of the remaining model coefficients. Also, other numerical methods for approximate posterior inference can be used, such as the integrated nested Laplace approximation [37] in the pursuit of further numerical robustness and efficiency. Both threshold-based and Integrated titers are invariant to specific classes of transformations of the dilution-killing curve. Threshold-based titers are invariant to transformations leaving unchanged the dilution associated to the critical killing value τ, whereas Integrated titers are invariant to multiplication of all non-negative killing values by the same non-negative constant. The strong linear relations between the posterior point estimates of threshold-based and Integrated titers shown in Figure 3.4 and 3.5 demonstrate that the estimated antibody functional activity is similar across the two titer definitions, although Integrated titers tend to provide more precise estimates. If titer invariance to multiplicative transformations of killing proved inadequate, different threshold-free titer definitions could be readily proposed. For instance, weighted averages of the minimum and maximum tested dilutions with weight proportional to interpretable killing statistics could provide alternative estimators of antibody functional activity. The parametric model used for simulation and analysis of experimental data is in our experience adequate to fit the observed OPKA curves. If non-linear heteroskedastic monotone models were found inadequate, for instance for the analysis of a large number of clinical data, flexible non-parametric Bayesian models centred at the current parametric likelihood using Dirichlet priors could be developed following [34]. A limitation to employing non-parametric models of the dilution-killing curve is that typically only a low number of serum dilutions are tested for each serum.

In this case, titer inferences may thus be sensitive to the value of the Dirichlet precision parameter. Also, in practice only experiments yielding a monotone dilution-killing pattern are deemed valid, making largely superfluous the development of non-monotone models for titer inference. Finally, a further limitation to using nonparametric models for titer inference is that the need for interpretable dilution-killing parameters is deeply ingrained in the current experimental practices, which have historically relied on biophysical dose-response models. From this perspective, the development of interpretable yet flexible non-linear dose-response models with identifiable parameters is a relevant and timely theme for further research in this field.

Chapter 4: Discussion of thesis results and ways forward.

Here an approach to bioassay quantification from serial dilution experiments using dimensionality reduction indices estimated from the viable portion of a dilution-killing curve was demonstrated. This approach is in essence different from the mainstream principles used for bioassay quantification, which are based on extrapolation of one dilution value at one fixed killing threshold. The strengths of the approach proposed here compared to the traditional approach are simply the result of the higher precision of estimators reflecting an aggregated behaviour along a curve compared to estimators of one value of the curve at a fixed point. This increased precision is reached both using a model free and a model approach. The first one is simple in its methodological foundation also for non-statisticians who can independently implement the method. Despite the simplicity of the methodological foundations of our approach, its acceptance in mainstream experimental work is currently being assessed, as its values in a large number of samples need being observed before a comprehensive opinion is crystallised. This assessment was welcome and taken as a healthy sanity check of methods that can be used for analyses as delicate as those performed on clinical trial samples.

The second approach preserves the same simple rationale and therefore at least the meaning is easy to understand. Its increased complexity from a methodological point of view make this method extremely interesting from the point of view of a researcher who have a strong quantitative background, but it becomes harder to implement for who have not programming knowledge.

Therefore the road for a wide acceptance of Integrated titers will be much longer but simultaneously more challenging.

Beyond the results illustrated here, some further research areas are being deepened. First, the computational robustness of T_I: in this paper MCMC algorithm that efficiently estimated Integrated titers was developed, however its complexity is an issue potentially limiting a wide understanding of the method proposed. Therefore the optimization of such algorithm exploring alternative methods, including adaptive MCMC algorithms, is currently under investigation. Second, a hybrid threshold free definition is being developed, which is a linear combination of the two definitions proposed in this thesis. The weight associated to each of these titer definitions reflects how well the dilution-killing model fits the data: if the model fits perfectly, then only the T_I estimator will be used, if it doesn't fit at all, then the T_f titers will be preferred. Third, estimation of threshold free and Integrated titers can be extended beyond the analysis of OPKA data. For instance the serum bactericidal assay [SBA, 38], which is used to measure the ability of serum antibody to kill gram-negative bacteria, represents an important experimental setup for further assessing the applicability of integrated titer definitions. Successful application of Integrated titers in this case would have particular relevance because SBA titers are the recognised immunological correlate of protection against meningicoccal diseases.

 In addition, threshold free titer definitions could be in principle used for non-functional immunoassay, such as Enzyme-Linked-Immunoassay (ELISA). In such cases, the assay features will pose new issue to further improve the current definitions. In the ELISA assay, the outcome (optical density) is bounded between 0 and 4. This additional constraint (finite lower bound) poses

additional challenges for the application of threshold-independent titer definitions, such as model selection and their biological interpretability.

References

1. A.K. Johri., L.C. Paoletti, P.Glaser, M. Dua, P.K. Sharma, G. Grandi and R.Rappuoli. Group B Streptococcus (2006): *global incidence and vaccine development.* Nat. Rev. Microbiology vol 4, no 12, pp 932-942.

2. Centers for Disease Control and Prevention. *Early-onset and late-onset neonatal group B streptococcal disease—United States, 1996-2004.* MMWR 2005;54(47): 1205-1208.

3. Gibbs,R.S., S. Schrag, and A. Schuchat (2004). *Perinatal infections due to group B streptococci.* Obstet Gynecol 104:1062-1076.

4. Edwards, M.S., and C.J. Baker (2005). *Group B streptococcal infections in elderly adults.* Clin Infect Dis **41**:839-847.

5. A. Schuchat, C. Whitney, K. Zangwill (1996). *Prevention of perinatal group B streptococcal disease: a public health perspective.* Morbid. Mortal. Weekly Rep, 1-24, vol.45 (RR-7).

6. S.Schrag, D.Phil, S.Zywicki, M.Farley, A.Reimgold, L.Harrison, L.Lewkovitz, J.Hadler, R.Danila, P.R.Cieslak, Anne Shuchat (2000): *Group B streptococcal disease in the era of intrapartum antibiotic prophilaxis.* New England Journal of Medicine, 15-20, vol.342

7. M.Moore, S.J.Schrag, A.Schuchat (2003): *Effects of intrapartum antimicrobialprophylaxis for prevention of Group B streptococcal disease on the incidence and ecology of early-onset neonatal sepsis.* The lancet: infectious Disease, 201-213, vol.3.

8. Baker, C. J., and D. L. Kasper (1976): *Correlation of maternal antibody deficiency with susceptibility to neo- natal group B streptococcal infection.*

New England Journal of Medicine, 752-756, vol.294.

9. Carol T. Baker (1990): *Immunization to prevent group B streptococcal diseases: victories and vexations*. The Journal of Infectious Diseases, 917-921, vol.161, no.5.

10. D.L.Kasper, L.C. Paoletti, M.R.Wessels,H.C.Guttormsen, V.J. Carey, H.J.Jennings, C,J.Baker (1996*) Immune response to type III Group B polysaccharide-Tetanus Toxoid Conjugate vaccine*. Journal of clinical investigation, vol 98, no 10, pp 2308-2314.

11. F.Y.C. Lin, L.E. Weisman,P.H.Azimi,J.B. Philips, P.Clark, J.Regan, G.G.Rhoads, C.E.Frasch, B.M. Gray, J.Troendle, R.A. Brenner,P.Moyer,J.D.Clemens (2004*). Level of maternal IgG anti Group B Streptococcus Type III antibody correlated with protections of Neonates against early-onset disease caused by the pathogen.* Journal of infectious disease, vol 190, no 5, pp 928-934.

12. F.Y.C. Lin, J.B. Philips III,P.H.Azimi, L.E.Weisman, P.Clark, G.C.Rhoads, J.Regan,N.F.Concepcion, C.E.Frasch,J.Troendle, R.A.Brenner, B.M. Gray,R.Bhushan, G.Fitzgerald,P.Moyer, and J.D.Clemens. Level of maternal antibody required to protect neonates against early onset disease caused by Group B Streptococcus type Ia: a multicenter, seroepidemiology study(2001). *Journal of infectious disease, vol 184, no 4, pp 1022-1028.*

13. D.Maione, I. Margarit, C.D. Rinaudo, V.Masignani, M.Mora, M.Scarselli, H.Tettelin, E.T.Iacobini, R.Rosini, N.D'Agostino, L.Miorin, S.Buccato, M.Mariani, G.Galli, R.Nogarotto, V.Nardi Dei, F.Vegni, C.Fraser, G.Mancuso, G.Teti, L.C.Madoff, L.C.Paoletti, R.Rappuoli, D.L.Kasper, J.L.Telford, G.Grandi (2005): *Identification of an universal group B Streptococcus vaccine by multiple genome screen.* Science, 148-150, vol.309, no.5731.

14. C.J.Baker, MA Rench, MS Edwards, RJ Carpenter, BM Hays, DL Kasper (1988*). Immunization of pregnant women with a polysaccharide vaccine of group B Streptococcus.* New England Journal of Medicine, 1180-1185, vol.319.

15. DL Kasper, L.C.Paoletti, MR Wessels, HK Guttormsen, V.J.Carey, H.J.Jennings, C.J.Baker (1996). *Immune response to type III group B streptococcal polysaccharide-tetanus toxoid conjugate vaccine.* Journal of Clinical Investigation, 2308-2314, vol.98, no.10.

16. C.J.Baker, MA Rench ,M.Fernandez, L.C.Paoletti, DL Kasper,MS Edwards (1999). *Safety and immunogenicity ofa bivalent group B streptococcal conjugate vaccine for serotype II and III.* Journal of Infectious diseases, 66-73, vol.181, issue 1.

17. *A.K Yetisen, M.S. Akram and C.R.Lowe (2013): Paper-based microfluidic point of care diagnostic devices.* The Royal society of chemistry. vol 13 ,pp 2210-2251

18. A.Voller, D.E. Bidwell and Ann Bartlett. *Enzyme immunoassays in diagnosti medicine:theory and practice.* Bull World Health Organ. 1976; 53(1): 55–65.

19. *C.P.Reinhart,M.J.Germain,E.V.Gronman,J.G.Mulhern,R.Kumar,D.E.Vaccaro (2008) : Functional immunoassay technology (FIT), a new approach for measuring physiological. functions: application of FIT to measure glomerular filtration rate (GFR).* American Journal of physiology vol195 no 5 pp 1583-1588.

20. E.Engvall and P.Pearlmann (1971): *Enzyme Linked Immunosorbent Assay (ELISA)* Quantitative Assay of Immunoglobulin G. Immunochemistry, *vol 8, 874-879.*

21. JH Mathews, PH Klesius, RA Zimmermen (1974). *Opsonin system of the group B Streptococcus.* Infection and Immunity, 1315-1320, vol.10, no.6.

22. MR Wessels, LC Paoletti, DL Kasper, JL Di Fabio, F.Michon, K.Holme, H.J.Jennings (1990). *Immunogenicity in animals of a polysaccharide-protein conjugate vaccine against type III group B Streptococcus.* Journal of Clinical Investigation, 1428-1433, vol.86, no.5.

23. L.M.Prescott: Microbioogy. *5th edition, 2002, pp 714-720*

24. R.S. Baltimore, D.L. Kasper, C.J. Baker, D.K. Goroff (1977). *Antigenic specificity of opsonophagocytic antibodies in rabbit anti-sera to group B streptococci. The Journal of Immunology vol 118 pp 673-678.*

25. M.S Edwards, C.J.Baker, D.L. Kasper (1979)*. Opsonic specificity of human antibody to the type III polysaccharide of group B Streptococcus*. The Journal of Infectious Diseases vol 140, 1004-1008.

26. H.K. Guttormsen, Y. Liu, L.C. Paoletti, 2008. *Functional activity of antisera to group B streptococcal conjugate vaccines measured with an opsonophagocytosis assay and HL-60 effector cells*. Human Vaccines vol 4, issue 5, 370-374.

27. sM.E. Halloran, I. Longini and C. Struchiner (2009). *Design and Analysis of Vaccine Studies*. Springer Monograph

28. P.G. Gottshalk, J.R. Dunn, (2005): *The five parameter logistic: A characterization and comparison with the four-parameter logistic.* Analytical Biochemistry 343 (54–65).

29. ICH Guidance for industry. *Validation of analytical procedures*. (Oct 21, 2010) *www.fda.gov./cder/Guidance/ichq2a.pdf*.

30. J.S. Liu: *Monte Carlo Strategies in Scientific computing* (2004). Springer series in statistics.

31. F.L. Ramsey (2005): *A Bayesian approach to bioassay*. Biometrics 28, 841-858.

32. L. Kuo (1983) *Bayesian Bioassay design*. The annals of statistics vol.11, issue no.3 886-895

33. P. Ramgopal, P. W. Laud and A. F. M. Smith ``*Nonparametric Bayesian bioassay with prior constraints on the shape of the potency curve''*. Biometrika (1993) 80 (3): 489-498.

34. A. E. Gelfand, L Kuo *Nonparametric Bayesian bioassay including ordered polytomous response*. Biometrika (1991) 78 (3): 657-666.

35. C. Ritz, C.J. Streibig (2005) *Bioassay Analysis using R*, Journal of statistical software; Vol.12, Issue.5.

36. S.P. Brooks, G.O. Roberts (1998) Assessing convergence of Markov chain Monte Carlo algorithms, Statistics and Computing.

37. H Rue,and H.Martino and N. Chopin (2009): *Approximate Bayesian inference for latent Gaussian models by using integrated nested Laplace approximations.* Journal of the Rojal Statistical Society:Series B (Statistical methodology) vol 71, pp391-392

38. R. Borrow, P. Balmer, E. Miller (2005): *Meningococcal Surrogates of Protection – Serum Bactericidal Assay Activity.* Clinical and Vaccine Immunology; vol 23 pp 2222-2227.

39. S.Romero-Steiner, C. Frasch, G. Carlone, R. Fleck, D.Goldblatt, and M. Nahms (2006). *Use of Opsonophagocytosis for Serological Evaluation of Pneumococcal Vaccines.* Clinical and Vaccine Immunology, vol 13 pp 165–169.

40. G. Siber, I. Chang, S.Baker, P.Fernsten, K. O'Brien, M. Santosham, K. Klugman, S. Madhi, P. Paradiso, and R. Kohberger (2007). *Estimating the protective concentration of anti-pneumococcal capsular polysaccharide antibodies.* Vaccines, vol 25 pp3816–3826

41. L. Verracchio, S. Romero-Steiner, J. Martinez, K. MacDonald, S. Barnard, T. Pilishvili, G. Carlone, D. Ambrosino, and D. Morline (2000). *Comparison of an Op- sonophagocytic assay and IgG ELISA to assess response to pneumococcal polysac- charide and pneumococcal conjugate vaccines in children and young adults with sickle cells disease.* Journal of Infectious disease vol 181 pp 1162–1166

42. J. Rodriguez-Granger, J. C. Alvargonzalez, A. Berardi, R. Berner, M. Kunze, M. Hufnagel, P. Melin, A. Decheva, G. Orefici, C. Poyart, J. Telford, A. Efstratiou, M. Killian, P. Krizova, L. Baldassarri, B. Spellerberg, A. Puertas, M. Rosa-Fraile (2012): *Prevention of group B streptococcal neonatal disease revisited. The DEVANI European project.* European Journal of Clinical Microbiological Infectious Diseases. vol 31 pp 2097–2104

Appendix: R code for estimation of Integrated titers

Here the R code written for estimating Integrated titers is reported in full, along with one example of titer inference from simulated data. This appendix demonstrates the computational complexity involved in titer estimation and the Author's efforts to provide numerically stable code ensuring the reproducibility of the results reported in this thesis. This code is currently not packaged into a user-friendly form and brief comments and interviewed below to the different computational routines. Efforts to present this code in a dedicated R package are currently ongoing.

```r
load(drc)
#set of dilutions considered for simulation
dilutions=c(30,120,480,1920,7680,30720)
seq = seq(min(dilutions),max(dilutions),5)

#parameter values for one simulation scenario
a = -2
d = 2
ys = -1
c=15000
b=4;
#corresponding Log-ratios and killings
Logratio<- d + (a-d)/((1+(dilutions/c)^b)^1)
killing=100*(1-2^ Logratio)
Logratio_seq<- d + (a-d)/((1+(seq/c)^b)^1)

#estimated "true" t50
t50  = c*(((a-d)/(ys-d))^(1/1) -1)^(1/b)

#first derivative of Logratio and killing
fprimox<-function(x,a,b,c,d,g){
 -((a-d)*g*b*(x)^(b-1))  /  (((1+(x/c)^b)^(g+1))*c^b)
}
#kprimo
kprimox=function(fprimo,LR){
-log(2)*fprimo*2^(LR)
}

#estimated "true" Integrated titers
NN=1000
rr = c(min(seq), max(seq[100*(1-2^Logratio_seq) > 0]))
difference = diff(rr)
un= seq(rr[1], rr[2], difference/NN)
LR = d + (a-d)/((1 + (un/c)^ b)^1)
kill_un = 100 * (1 - 2^(LR))
kprime = abs(kprimox(fprimox(un, a,b,c,d, 1), LR))
cons = diff(rr) * mean(kill_un * kprime)
tInt = diff(rr) * mean(un * kill_un * kprime)/(cons)
```

```r
#
Niter=2000 #number of simulation
ldil=length(dilutions)

#simulation of Logratio data
LR4dil_s1=matrix(0,Niter,ldil)
h=30000# h values for this scenario
sds_4PL_dil = h*fprimox(dilutions,a,b,c,d,1)#first derivative of
 dilution-logratio curve
kk = matrix(0,Niter,1)

for(i in 1:Niter){
 COND = 0
 aaa = 0
 while(COND < 1){
        LR4dil_s1[i,]=rnorm(ldil,Logratio,sds_4PL_dil)
        COND = (sum(diff(LR4dil_s1[i,])<0)==0) #monotone data
        aaa=aaa+1
 }
 kk[i,1]=aaa
}


#likelihood model
 loglik4pl_optim = function(par,dilution,logratio,msds){
 rrr = 0
 for(i in 1:dim(logratio)[[1]]){
            fpl = par[4] + (par[1]-
par[4])/(1+((dilution[i,]/par[3])^par[2]))

      sds=par[5]*abs(fprimox(dilution[i,],par[1],par[2],par[3],par[4
],1) )
            sds = apply(t(as.matrix(sds)),2,max,msds)
             # Log-likelihood
        rrr = rrr+sum(dnorm(logratio[i,],fpl,sds,log=TRUE))
    }
    if(is.na(rrr)==1 | is.infinite(rrr)==1 | par[5]<=0 | par[3]<=0)
 rrr = -.Machine$double.xmax # numerical patch
    return(rrr)
 }

#function for MLE estimates of parameters likelihood

estimate_4pl_optim=function(fivep_dil,dil,h_0,msds) {

coef=matrix(0,1,6)
dimnames(coef)[[2]]=list("b","d","a","c","g","h")

 coef[1,1:4]=coef(drm(as.vector(fivep_dil)~as.vector(dil),fct=LL.4())
 )

 a=coef[1,3]#d
 b=coef[1,1]#b
 c=coef[1,4]#e
 d=coef[1,2]#c
 g=1#f
 coef[1,5]=1

par=c(a,b,c,d,h_0)
fit=optim(par,
```

```
 loglik4pl_optim,logratio=t(as.matrix(c(fivep_dil))),msds=msds,
 dilution=t(as.matrix(c(dil))),lower=0,upper=1000,method="L-BFGS-B")


coef[1,6]=fit$par[5]
list(par,c(fit$par[1:4],g,fit$par[5]),fit$convergence)



}


#MCMC algorhitm
mcmc4PLcu <- function(dilution,
 logratio,mu_0,sigma_0,coeff_0,sigma_q,N,sss,NN,sw,msds){

 if(max(100*(1-2^logratio)) <0|| min(100*(1-2^logratio))>50
 ){coeffs = matrix(-1000,N,9)}

 else{
 i=1
 coeffs = matrix(0,N,9)  # a,b,d,c,h,loglik,tINT,t504PL,tINT2 (one
 additional titer definition)
 coeffs_prop = matrix(0,N,5)

 coeffs_prop[i,1:3] = rnorm(3,coeff_0[1:3],sigma_q[1:3])
 coeffs_prop[i,4:5] = rlnorm(2,log(coeff_0[4:5]),sigma_q[4:5])

 if(sum(coeff_0)!=0){
       coeffs[i,1:5]=coeff_0
 }
 else{
       coeffs[i,1:3] = rnorm(3,mu_0[1:3],sigma_0[1:3]) # a,b,d
       coeffs[i,4:5] = rlnorm(2,mu_0[4:5],sigma_0[4:5]) # c,h
 }

LR4p_1 <- coeffs[i,3] + (coeffs[i,1] - coeffs[i,3])/((1 +
(sss/coeffs[i,4])^ coeffs[i,2])^1)
Kil4p_1 = 100 * (1 - 2^(LR4p_1))

     if (max(Kil4p_1)>50){

        rr_4Pl_1 = c(min(sss), max(sss[Kil4p_1 > 0]))
        d_rr_4Pl_1 = diff(rr_4Pl_1)
        un_4Pl_1 = seq(rr_4Pl_1[1], rr_4Pl_1[2],d_rr_4Pl_1/NN)

        LR_un_4Pl_1 = coeffs[i,3] + (coeffs[i,1] - coeffs[i,3])/((1 +
(un_4Pl_1/coeffs[i,4])^ coeffs[i,2])^1)
        kill_un_4Pl_1 = 100 * (1 - 2^(LR_un_4Pl_1))

        #integrated titer 4PL kk'
        kprime_4Pl_1 = abs(kprimox(fprimox(un_4Pl_1, coeffs[i,1],
coeffs[i,2], coeffs[i,4], coeffs[i,3], 1), LR_un_4Pl_1))

        C_un_4Pl_kprime_1 = diff(rr_4Pl_1) * mean(kill_un_4Pl_1 *
kprime_4Pl_1)

        coeffs[i,7] = diff(rr_4Pl_1) * mean(un_4Pl_1 * kill_un_4Pl_1 *
kprime_4Pl_1)/(C_un_4Pl_kprime_1)

        # closed form expression for t504PL, conditional on estimated
coeffs
        coeffs[i,8]=coeffs[i,4]*(((coeffs[i,1]-coeffs[i,3])/(ys-
```

```r
coeffs[i,3]))^(1/1) -1)^(1/coeffs[i,2])

#integrated titer 4PL kk' second version
w = C_un_4Pl_kprime_1/kill_un_4Pl_1[1]
coeffs[i,9]= rr_4Pl_1[2]*w + rr_4Pl_1[1]*(1-w)


}
else {

        coeffs[i,7]= NA
        coeffs[i,8]= NA
        coeffs[i,9]= NA

}

loglik_cur =
loglik4pl_optim(c(coeffs[i,1],coeffs[i,2],coeffs[i,4],coeffs[i,3],co
effs[i,5]), dilution ,logratio,msds)

coeffs[i,6]=loglik_cur

uu = log(runif(N,0,1))

for(i in 2:N){

        logpro_diff = matrix(0,1,5)
        if(sw==0){ # random walk proposal

                # plain RW proposal
                coeffs_prop[i,1:3] = rnorm(3,coeffs_prop[i-
1,1:3],sigma_q[1:3])
                coeffs_prop[i,4:5] = rlnorm(2,log(coeffs_prop[i-
1,4:5]),sigma_q[4:5])

        }
        else    { # independent sampler proposal
                coeffs_prop[i,1:3] = rnorm(3,coeff_0[1:3],sigma_q[1:3])
                coeffs_prop[i,4:5] =
rlnorm(2,log(coeff_0[4:5]),sigma_q[4:5])

                logpro_diff[1:3] = dnorm(coeffs_prop[i-
1,1:3],coeff_0[1:3],sigma_q[1:3],log=TRUE)-
dnorm(coeffs_prop[i,1:3],coeff_0[1:3],sigma_q[1:3],log=TRUE)

                logpro_diff[4:5] = dnorm(log(coeffs_prop[i-
1,4:5]),log(coeff_0[4:5]),sigma_q[4:5],log=TRUE)-
dnorm(log(coeffs_prop[i,4:5]),log(coeff_0[4:5]),sigma_q[4:5],log=TRU
E)            # c,h
        }

        # a,b,d
        logpri_diff = matrix(0,1,5)

        logpri_diff[1:3] =
dnorm(coeffs_prop[i,1:3],mu_0[1:3],sigma_0[1:3],log=TRUE)-
dnorm(coeffs[i-1,1:3],mu_0[1:3],sigma_0[1:3],log=TRUE)

        #c,h
        logpri_diff[4:5] =
dnorm(log(coeffs_prop[i,4:5]),mu_0[4:5],sigma_0[4:5],log=TRUE)-
dnorm(log(coeffs[i-1,4:5]),mu_0[4:5],sigma_0[4:5],log=TRUE)
```

```r
        # print(dnorm(log(coeffs[i-
1,4:5]),mu_0[4:5],sigma_0[4:5],log=TRUE))
        #
print(dnorm(log(coeffs_prop[i,4:5]),mu_0[4:5],sigma_0[4:5],log=TRUE)
)
        # print(coeffs_prop[i,4:5])
        # print(logpro_diff)
        # print(logpri_diff)
# #          print(coeffs_prop[i,])

 # component-wise update

  # recompute likelihood because the data have changed
  loglik_cur = loglik4pl_optim(c(coeffs[i-1,1],coeffs[i-
1,2],coeffs[i-1,4],coeffs[i-1,3],coeffs[i-
1,5]),dilution,logratio,msds)

# update coefficient a
loglik_prop = loglik4pl_optim(c(coeffs_prop[i,1],coeffs[i-
1,2],coeffs[i-1,4],coeffs[i-1,3],coeffs[i-
1,5]),dilution,logratio,msds)

loglik_diff = loglik_prop-loglik_cur #

    #print(loglik_diff)

acc_a = (uu[i]<=loglik_diff+logpri_diff[1]+logpro_diff[1]) # do MCMC
coeffs[i,1] = coeffs_prop[i,1]*acc_a + (1-acc_a)*coeffs[i-1,1]
loglik_cur=loglik_prop*acc_a + (1-acc_a)*loglik_cur

# update coefficient b
loglik_prop =
loglik4pl_optim(c(coeffs[i,1],coeffs_prop[i,2],coeffs[i-
1,4],coeffs[i-1,3],coeffs[i-1,5]),dilution,logratio,msds)

#       print(loglik_diff)

acc_b = (uu[i]<=loglik_diff+logpri_diff[2]+logpro_diff[2]) # do MCMC
coeffs[i,2] = coeffs_prop[i,2]*acc_b + (1-acc_b)*coeffs[i-1,2]
loglik_cur=loglik_prop*acc_b + (1-acc_b)*loglik_cur

# update coefficient c
loglik_prop =
loglik4pl_optim(c(coeffs[i,1],coeffs[i,2],coeffs_prop[i,4],coeffs[i-
1,3],coeffs[i-1,5]),dilution,logratio,msds)

 loglik_diff = loglik_prop-loglik_cur
#print(loglik_diff)

acc_c = (uu[i]<=loglik_diff+logpri_diff[4]+logpro_diff[4]) # do MCMC
coeffs[i,4] = coeffs_prop[i,4]*acc_c + (1-acc_c)*coeffs[i-1,4]
loglik_cur=loglik_prop*acc_c + (1-acc_c)*loglik_cur

# update coefficient d
loglik_prop =
loglik4pl_optim(c(coeffs[i,1],coeffs[i,2],coeffs[i,4],coeffs_prop[i,
3],coeffs[i-1,5]),dilution,logratio,msds)

 loglik_diff = loglik_prop-loglik_cur
#print(loglik_diff)
```

```r
acc_d = (uu[i]<=loglik_diff+logpri_diff[3]+logpro_diff[3]) # do MCMC
coeffs[i,3] = coeffs_prop[i,3]*acc_d + (1-acc_d)*coeffs[i-1,3]
loglik_cur=loglik_prop*acc_d + (1-acc_d)*loglik_cur

# update coefficient h
loglik_prop =
loglik4pl_optim(c(coeffs[i,1],coeffs[i,2],coeffs[i,4],coeffs[i,3],co
effs_prop[i,5]),dilution,logratio,msds)

loglik_diff = loglik_prop-loglik_cur
#print(loglik_diff)

acc_h = (uu[i]<=loglik_diff+logpri_diff[5]+logpro_diff[5]) # do MCMC
coeffs[i,5] = coeffs_prop[i,5]*acc_h + (1-acc_h)*coeffs[i-1,5]
loglik_cur=loglik_prop*acc_h + (1-acc_h)*loglik_cur

coeffs[i,6] = loglik_cur

acc_all = acc_a+acc_b+acc_c+acc_d+acc_h

if(sum(is.na(acc_all))==0) {

if(acc_all>0){
            LR4p_1 <- coeffs[i,3] + (coeffs[i,1] - coeffs[i,3])/((1
+ (sss/coeffs[i,4])^ coeffs[i,2])^1)
            Kil4p_1 = 100 * (1 - 2^(LR4p_1))

             if(max(Kil4p_1)<50){
                    coeffs[i,7]= NA
                    coeffs[i,8]= NA
                    coeffs[i,9]= NA
                    }
                    else{

    rr_4Pl_1 = c(min(sss), max(sss[Kil4p_1 > 0]))
    d_rr_4Pl_1 = diff(rr_4Pl_1)
    un_4Pl_1 = seq(rr_4Pl_1[1], rr_4Pl_1[2],d_rr_4Pl_1/NN)
    LR_un_4Pl_1 = coeffs[i,3] + (coeffs[i,1] - coeffs[i,3])/((1 +
(un_4Pl_1/coeffs[i,4])^ coeffs[i,2])^1)
    kill_un_4Pl_1 = 100 * (1 - 2^(LR_un_4Pl_1))

    #integrated titer 4PL kk', set 1
    kprime_4Pl_1 = abs(kprimox(fprimox(un_4Pl_1, coeffs[i,1],
coeffs[i,2], coeffs[i,4], coeffs[i,3], 1), LR_un_4Pl_1))

    C_un_4Pl_kprime_1 = d_rr_4Pl_1 * mean(kill_un_4Pl_1 *
kprime_4Pl_1)
    coeffs[i,7] = d_rr_4Pl_1 * mean(un_4Pl_1 * kill_un_4Pl_1 *
kprime_4Pl_1)/(C_un_4Pl_kprime_1)

    logratiop <- coeffs[i,3] + (coeffs[i,1] - coeffs[i,3])/((1 +
(dilution/coeffs    [i,4])^ coeffs[i,2])^1)

    # closed form expression for t50PL conditional on estimated
coeffs
     coeffs[i,8]=coeffs[i,4]*(((coeffs[i,1]-coeffs[i,3])/(ys-
coeffs[i,3]))^(1/1) -1)^(1/coeffs[i,2])

    #integrated titer 4PL kk' second version
w = C_un_4Pl_kprime_1/kill_un_4Pl_1[1]
```

```r
  coeffs[i,9]= rr_4Pl_1[2]*w + rr_4Pl_1[1]*(1-w)


        }
          }
        else{
                coeffs[i,7]=coeffs[i-1,7]
                coeffs[i,8]=coeffs[i-1,8]
                coeffs[i,9]=coeffs[i-1,9]
        }
 }
 else{
        coeffs[i,7]=coeffs[i-1,7]
        coeffs[i,8]=coeffs[i-1,8]
        coeffs[i,9]=coeffs[i-1,9]
 }
}
 }
 return(coeffs)
}




#empty matrices required for titer simulation
fits4dil = matrix(0,Niter,7)
N=2000#number of MCMC iteration
msds=0.005#constant to prevent numerical issues (defined in
 likelihood)
bnin = 1
coeff=array(matrix(1,N,9),c(N,9,Niter))#matrix with estimates of
 a,b,c,d,h,likelihood value, t50 and tInt
t_Int_sim=matrix(0,Niter,1)
t_50_sim=matrix(0,Niter,1)
CV_sim_t50=matrix(0,Niter,1)
CV_sim_tInt=matrix(0,Niter,1)
mu_0=c(1.4, -2.4 ,-4.7 , 7.4 , 4.2)#prior means distribution (from
 charachterization data)
par4PL_est_b=matrix(0, Niter,5)#bayesian estimates of likelihood
 parameters
par4PL_est_mle=matrix(0, Niter,5)#maximum likelihood estimates of
 likelihood parameters
arate_Int = matrix(0,dim(coeff)[3],N-1) # acceptance rates for
 Integrated titers (each simulation)
arate_50 = matrix(0,dim(coeff)[3],N-1) #acceptance rates for T50
 titers (each simulation)
sigma_0=c(0.8,1.3,1,1.4,0.5)#starting values for MCMC
sigma_q = c(0.2,0.2,0.2,0.1,0.1)#starting values for MCMC
NN=2000
sw=1#use independent sampler
```

**#run the 2000 simulations for estimating t50 and tInt using MCMC
 function (one chain-independent sampler component-wise update)**

```r
da1 = date()
for(i in 1:Niter){

  stimadil=estimate_4pl_optim(LR4dil_s1[i,],dilutions,h,msds)

  fit4PLdil = unlist(stimadil[2])##
  par4PL_est_mle[i,] = fit4PLdil[c(1:4,6)]

  coeff_0 = c(fit4PLdil[1], fit4PLdil[2], fit4PLdil[4], fit4PLdil[3],
```

```
  fit4PLdil[6])
  coeff[,,i]=
mcmc4PLcu(t(as.matrix(dilutions)),t(as.matrix(LR4dil_s1[i,])),mu_0,s
igma_0,coeff_0,sigma_q/6,N,seq,NN,sw,msds)

  t_Int_sim[i,]= median(coeff[bnin:N,7,i],na.rm=T)
  t_50_sim[i,]= median(coeff[bnin:N,8,i],na.rm=T)

CV_sim_t50[i,]=sd(coeff[bnin:N,8,i],na.rm=T)/mean(coeff[bnin:N,8,i],
na.rm=T)

CV_sim_tInt[i,]=sd(coeff[bnin:N,7,i],na.rm=T)/mean(coeff[bnin:N,7,i]
,na.rm=T)
  par4PL_est_b[i,]=apply(coeff[bnin:N,1:5,i],2, mean,na.rm=T) #

arate_Int[i,1:(sum(is.na(coeff[,7,i])==F)-1)] = cumsum(diff(coeff[,
7,i][is.na(coeff[,7,i])==F])>0)/(1:(length(coeff[,7,i][is.na(coeff[,
7,i])==F])-1)) # HERE
arate_50[i,1:(sum(is.na(coeff[,8,i])==F)-1)] =
cumsum(diff(coeff[,8,i][is.na(coeff[,8,i])==F])>0)/(1:(length(coeff[
,8,i][is.na(coeff[,8,i])==F])-1)) # HERE

print(i)
}
da2 = date()
rbind(da1,da2)

t_simdil_Dec =data.frame(cbind( t_50_sim,t_Int_sim, CV_sim_t50,
CV_sim_tInt))

#typical plot to assess relationship and precision of TI and T50
plot(t_simdil_Dec $t_50_sim, t_simdil_Dec
$t_Int_sim,xlim=c(3000,20000),ylim=c(3000,20000),xlab="Threshold
based titers",ylab="Integrated titers",main="scenario X
titers",cex.main=1.8,cex.lab=1.5,cex=1.5,cex.axis=1.3)
abline(0,1)
plot(100*(t_simdil_Dec $CV_sim_t50), 100*(t_simdil_Dec
$CV_sim_tInt),ylim=c(0,8),xlim=c(0,8),xlab="Threshold based
titers",ylab="Integrated
titer",cex.main=1.8,cex.lab=1.5,main="Scenarion X
CV%",cex=1.5,cex.axis=1.3)
abline(0,1)
```